

UC Davis

UC Davis Previously Published Works

Title

Ozone Production in the Soberanes Smoke Haze: Implications for Air Quality in the San Joaquin Valley During the California Baseline Ozone Transport Study

Permalink

<https://escholarship.org/uc/item/4f3144mk>

Journal

Journal of Geophysical Research: Atmospheres, 125(11)

ISSN

2169-897X

Authors

Langford, Andrew O
Alvarez, Raul J
Brioude, J
[et al.](#)

Publication Date

2020-06-16

DOI

10.1029/2019jd031777

Peer reviewed

JGR Atmospheres

RESEARCH ARTICLE

10.1029/2019JD031777

Key Points:

- Aircraft and remote sensing measurements are used to investigate impacts of the Soberanes Fire on air quality in the San Joaquin Valley
- Ozone enhancements in excess of 50 ppbv were measured by both lidar and aircraft between 1 and 3 km above the surface
- No significant enhancements in surface ozone were observed

Supporting Information:

- Supporting Information S1
- Figure S1

Correspondence to:

A. O. Langford,
andrew.o.langford@noaa.gov

Citation:

Langford, A. O., Alvarez, R. J., II, Brioude, J., Caputi, D., Conley, S. A., Evan, S., et al. (2020). Ozone production in the Soberanes smoke haze: Implications for air quality in the San Joaquin Valley during the California Baseline Ozone Transport Study. *Journal of Geophysical Research: Atmospheres*, 125, e2019JD031777. <https://doi.org/10.1029/2019JD031777>

Received 4 OCT 2019

Accepted 9 APR 2020

Accepted article online 21 APR 2020

Author Contributions:

Data curation: Christoph J. Senff, Emma L. Yates




Investigation: Raul J. Alvarez IIDani Caputi, Stephen A. Conley, S. Evan, Ian C. Faloona, Laura T. Iraci, Guillaume Kirgis, Josette E. Marrero, Ju-Mee Ryoo, Christoph J. Senff, Emma L. Yates

Resources: J. Brioude

Writing – review & editing: Raul J. Alvarez II Ian C. Faloona, Laura T. Iraci, Christoph J. Senff, Emma L. Yates

©2020. This article has been contributed to by US Government employees and their work is in the public domain in the USA.

Ozone Production in the Soberanes Smoke Haze: Implications for Air Quality in the San Joaquin Valley During the California Baseline Ozone Transport Study

Andrew O. Langford¹ , Raul J. Alvarez II¹, J. Brioude², Dani Caputi³, Stephen A. Conley⁴, S. Evan², Ian C. Faloona³ , Laura T. Iraci⁵ , Guillaume Kirgis^{1,6}, Josette E. Marrero^{5,7}, Ju-Mee Ryoo^{5,8}, Christoph J. Senff^{1,6}, and Emma L. Yates^{5,9}

¹NOAA Earth System Research Laboratories/Chemical Sciences Laboratory, Boulder, CO, USA, ²Laboratoire de l'Atmosphère et des Cyclones (LACy), UMR 8105, CNRS, Université de La Réunion, Météo-France, Saint-Denis, France, ³Department of Land, Air, and Water Resources, University of California, Davis, CA, USA, ⁴Scientific Aviation, Inc., Boulder, CO, USA, ⁵Atmospheric Science Branch, NASA Ames Research Center, Moffett Field, CA, USA, ⁶Cooperative Institute for Research in Environmental Sciences, University of Colorado, Boulder, CO, USA, ⁷Now at Sonoma Technology, Inc., Petaluma, CA, USA, ⁸Science and Technology Corporation, Moffett Field, CA, USA, ⁹Bay Area Environmental Research Institute, Petaluma, CA, USA

Abstract The Soberanes Fire burned 53,470 ha (132,127 acres) along the central California coast between 22 July and 12 October 2016, generating dense smoke and a variety of gaseous compounds that drifted eastward into the San Joaquin Valley Air Basin (SJVAB), an “extreme” nonattainment area for ozone (O₃). These gases included nitrogen oxides (NO_x) and volatile organic compounds, the photochemical precursors of O₃. The fire started during the California Baseline Ozone Transport Study, a field campaign that brought aircraft, surface, and remote sensing measurements of O₃ and related species to central California. In this paper, we use the California Baseline Ozone Transport Study measurements to assess the impact of the Soberanes Fire on ozone and particulate air quality in the SJVAB. We focus our analysis on 27 July to 2 August when the smoke haze was heaviest and the highest O₃ concentrations in the SJVAB during 2016 were recorded. Our analyses suggest that while 40 to 60 ppbv of fire-generated O₃ was transported to the eastern SJVAB in the 1- to 3-km-altitude range, relatively little smoke or fire-generated O₃ reached the surface in the Visalia area.

1. Introduction

The adverse impacts of wildfire smoke on human health and welfare in the western United States and Canada have grown as long-standing fire suppression practices and climatic shifts have contributed to increased wildfire activity across the region (Bryant & Westerling, 2014; Westerling et al., 2016). The health impacts are of particular concern in California where many of the state's 40 million residents have been exposed to wildfire smoke in recent years (Kochi et al., 2012, 2016). An analysis by Wettstein et al. (2018) showed statistically significant increases in emergency room visits by the elderly for heart attack (15%), stroke (22%), and respiratory complaints (18%) on dense smoke days across northern and central California during the 2015 fire season, when nearly 323,000 ha (800,000 acres) burned across the state. The potential health effects have only increased since that time with 766,000 ha (1.9 million acres) burned in 2018, the most destructive fire season in California history (<https://www.nifc.gov/>). Smoke from these fires impacted rural and urban areas alike, with daily average fine particulate (PM_{2.5}) concentrations reaching 250 and 177.5 μg/m³ in Sacramento and San Francisco, respectively, when smoke from the devastating 62,052 ha (153,336 acre) Camp Fire in Paradise drifted westward from the Sierra Nevada foothills in mid-November. These daily averages are more than 5 times the U.S. National Ambient Air Quality Standard (NAAQS) of 35 μg/m³ established by the U.S. Environmental Protection Agency (EPA) to protect human health and welfare.

In addition to smoke, wildfires generate a variety of gaseous compounds including nitrogen oxides (NO + NO₂ = NO_x), carbon monoxide (CO), methane (CH₄), and other volatile organic compounds that

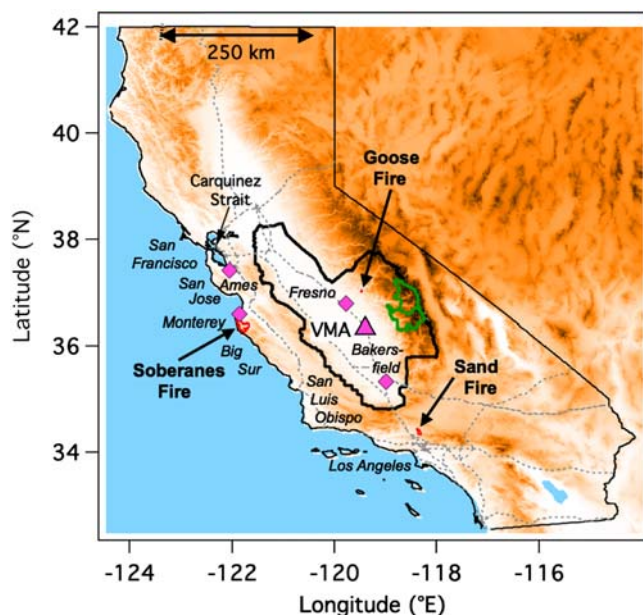


Figure 1. Shaded relief map of California and Nevada with the San Joaquin Valley Air Basin outlined in black. The basin is bounded by the Sierra Nevada Mountains to the east and the various Coast and Transverse Ranges to the west and south, respectively. The Kings Canyon and Sequoia National Parks are outlined in green and the Soberanes, Goose, and Sand Fire burn areas in red. The magenta triangle represents the Visalia Municipal Airport (VMA), and the diamonds show the Bakersfield, Fresno, Monterey, and Ames AERONET sites, respectively.

are the photochemical precursors of ozone (O_3). Ozone has also been linked to increased morbidity and mortality (U.S. Environmental Protection Agency, 2014) as well as damage to growing vegetation (Avnery et al., 2011a, 2011b) and is a long-standing problem in the South Coast and San Joaquin Valley Air Basins (SoCAB and SJVAB, respectively) of California, which are currently designated “extreme” ozone (O_3) nonattainment areas (<https://www.epa.gov/green-book>). Wildfires can contribute significantly to ambient surface concentrations across the western United States (Jaffe et al., 2008; Pfister et al., 2008), and O_3 produced above the boundary layer can be transported thousands of kilometers downwind to impact surface O_3 concentrations in the eastern United States (Wotawa & Trainer, 2000). Quantifying these contributions is difficult, however, since the amount of O_3 generated in wildfire plumes is highly variable and depends not only on temperature, humidity, and solar flux, which drive the photochemical production rates, but also on the plume injection height and precursor emissions rates that depend in turn on poorly quantified parameters such as fuel type and moisture content, combustion efficiency, and local meteorology (Jaffe & Wigder, 2012).

In this paper, we use airborne, surface, and remote sensing measurements made during the 2016 California Baseline Ozone Transport Study (CABOTS) (Faloona et al., 2020) to examine the production of O_3 in the Soberanes Fire plume and estimate the impact on surface O_3 concentrations in the SJVAB during the summer of 2016. This fire, which burned more than 52,600 ha (130,000 acres) along the central California coast between 22 July and 12 October 2016, created an elevated smoke haze that covered the southern and central SJVAB in late July and early August. We

focus our analysis on late July and early August when the smoke haze was most pervasive and the highest surface O_3 concentrations in the SJVAB during 2016 were recorded. We augment the CABOTS lidar and aircraft data with measurements from in situ regulatory monitors (www.arb.ca.gov) and the Aerosol Robotic Network (AERONET) (Holben et al., 1998) and use NASA Moderate Resolution Imaging Spectroradiometer (MODIS) satellite imagery in conjunction with the FLEXPART and HYSPLIT models to track the dispersion of the Soberanes Fire plume. Correlations between O_3 , CH_4 , and CO_2 from the aircraft measurements, and aerosol backscatter and O_3 from the lidar retrievals (see the supporting information) are used to estimate the amount of fire-generated O_3 in the elevated smoke haze. Our analyses show that while the fire plume increased O_3 by 40 to 60 ppbv between 1 and 3 km above the SJVAB, the impact of the smoke and excess O_3 on surface air quality in the eastern SJVAB was minimal.

2. The California Baseline Ozone Transport Study

The CABOTS field campaign (Faloona et al., 2020) was organized by the California Air Resources Board to investigate the contributions of background O_3 originating from Asian pollution (Lin, Fiore, Horowitz et al., 2012) and stratospheric intrusions (Lin, Fiore, Cooper et al., 2012) on surface concentrations in the SJVAB (Figure 1). The study was conducted between late May and mid-August of 2016 with two intensive operating periods (IOP1: 27 May to 18 June and IOP2: 18 July to 7 August). A primary goal of CABOTS was the characterization of O_3 above the SJVAB, and the measurements included daily profiling of O_3 and aerosol backscatter by the National Oceanic and Atmospheric Administration (NOAA)/Earth System Research Laboratory TOPAZ (Tunable Optical Profiler for Aerosols and oZone) mobile differential absorption lidar system (Alvarez et al., 2011) from the Visalia Municipal Airport (VMA, 36.315°N, -119.392°E, 88 m above sea level, asl) during the two IOPs. Visalia is located about one third of the way from Fresno to Bakersfield, the two most populous cities in the San Joaquin Valley (SJV), and the TOPAZ lidar was collocated with a radar wind profiler and Radio Acoustic Sounding System operated by the San Joaquin Valley Air Pollution Control District (Bao et al., 2008) and a vertically staring Doppler lidar operated by NOAA.

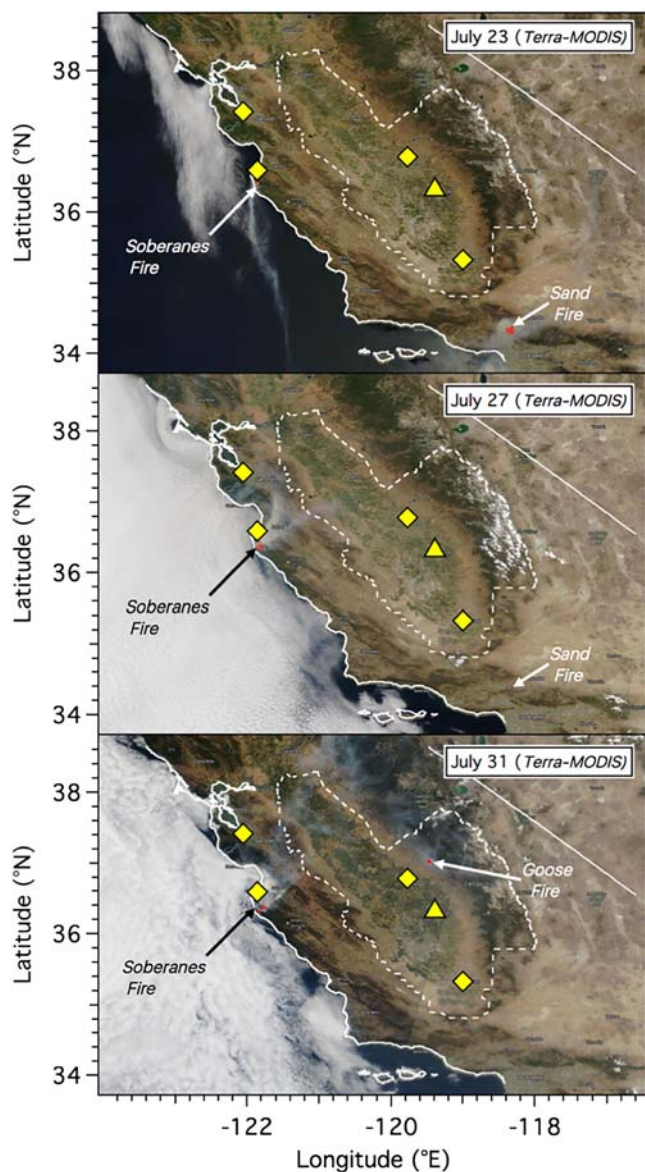


Figure 2. Terra-MODIS images (~1030 Pacific Daylight Time, PDT) from (top to bottom) 23, 27, and 31 July. The small red triangles show the MODIS Fires and Thermal Anomalies detections from the Soberanes, Sand, and Goose Fires. The SJVAB is outlined in dotted white. The yellow triangle and diamonds mark the VMA and AERONET sites, respectively.

Zhong et al., 2004). The thermal contrast between the cold ocean water and warm land surfaces creates a pressure gradient that forces clean marine air through the Carquinez Strait (cf. Figure 1) and up the valley during the day, bringing with it a variety of pollutants including the NO_x and volatile organic compound precursors of O_3 from the densely populated San Francisco Bay Area. This ~1-km-deep inflow also entrains urban emissions from Fresno and other regional cities and from dispersed transportation, agricultural, and petrochemical sources as it moves up the valley toward Bakersfield (Pusede & Cohen, 2012; Pusede et al., 2014).

The Pacific inflow is amplified by thermally driven up-valley winds that are modulated by daytime upslope flows along the flanks of the Sierra Nevada Mountains to the east and Coast Ranges to the west. Widespread agricultural irrigation (Li et al., 2016) and subsidence created by the mountain-valley circulations and persistent North Pacific High (Trousdell et al., 2016) typically cap the afternoon mixed layers below 1 km

Ozone, CO_2 , CH_4 , and other species were also sampled by single-engine Mooney TLS Bravo and Ovation 2 research aircraft operated by the University of California, Davis (UC Davis) and Scientific Aviation (SciAv) (Trousdell et al., 2019) and by the NASA Alpha Jet Atmospheric eXperiment (AJAX) research aircraft (Yates et al., 2015). Details of the sampling techniques and intercomparisons between the lidar and airborne O_3 measurements are described in Leblanc et al. (2018) and Langford et al. (2019).

3. The Soberanes Fire

The Soberanes Fire started on the morning of Friday, 22 July 2016, 4 days after the beginning of the second CABOTS IOP. It spread from an illegal campfire in Garrapata State Park near Big Sur and Monterey (cf. Figure 1) and burned 53,470 ha (132,127 acres) of grasslands, oak woodlands, chaparral, mixed hardwood/conifer, coast redwood, and coastal scrub between sea level and about 1,500 m asl over the next 10 weeks (National Interagency Coordination Center, 2017). Potter (2016) divided the evolution of the fire into three stages, with the end of the first stage (22 July to 7 August) coinciding with the conclusion of the second CABOTS IOP. This period was characterized by high ambient temperatures, clear skies, and unusually dry conditions, and the fire expanded rapidly with a mean burn rate of ~1,375 ha (3,400 acres) per day. More than 23,269 ha (57,500 acres) or 40% of the total burn area was scorched during this roughly 2-week period, with 13,326 ha (32,930 acres) and 57 homes burned in the first 7 days (22–29 July).

Two other wildfires affected the SJVAB during the second CABOTS IOP. The Sand Fire in Los Angeles County also started on 22 July and grew rapidly to cover more than 8,094 ha (20,000 acres) by the following evening (<https://www.fire.lacounty.gov>). This fire was 85% contained at 15,731 ha (38,873 acres) by the morning of 29 July and 100% contained at 16,767 ha (41,432 acres) on 3 August. The much smaller Goose Fire started in the Sierra foothills east of Fresno on the afternoon of 30 July and was fully extinguished on 9 August (<https://www.fire.ca.gov/incidents/2016/7/30/goose-fire/>). This fire burned nearly 728 ha (1,800 acres) of grass, scrub, and oak woodlands over the first 24 hr but was attacked aggressively and did not spread beyond 907 ha (2,241 acres).

4. Dispersion of Smoke Into the SJV

The dispersion of Soberanes smoke into the SJVAB was accomplished primarily by the thermally driven circulations that dominate the regional transport in summer when the synoptic forcing is weak (Bao et al., 2008;

(Bianco et al., 2011), and some of the pollution carried into the mountains by the afternoon upslope winds (Panek et al., 2013) is recirculated back over the valley above the shallow boundary layers (De Young et al., 2005; Fast et al., 2012; Gohm et al., 2009; Rampanelli et al., 2004; Zardi & Whiteman, 2013). There, the pollution accumulates in a persistent “buffer layer” (Faloona et al., 2020; Trousdell et al., 2019) that can persist for days or even weeks until dispersed by passing cold frontal systems. During CABOTS, free tropospheric air flowing over the Coast Ranges also carried smoke from the Soberanes Fire into the buffer layer where it mingled with the anthropogenic pollution.

The Soberanes Fire emissions were initially trapped by the coastal inversion, and the *Terra-MODIS* image from 23 July (Figure 2, top panel) shows the nascent smoke plume streaming southward over the Pacific Ocean. Some of the emissions were lofted higher as the fire grew, and the image from 27 July shows smoke flowing inland with the southwesterly winds aloft (Figure 2, middle panel). Smoke continued to drift inland over the next several days, and the *Terra-MODIS* image from 31 July shows the Soberanes plume mingling with smoke from the Goose Fire. Smoke from the Sand Fire is also visible in the 23 July image, but not the images from 27 and 31 July.

Figure 3 plots FLEXPART biomass burning CO tracer distributions (see the supporting information) on the 900 hPa (~1 km asl), 850 hPa (~1.5 km asl), and 700 hPa (~3.1 km asl) surfaces corresponding to the *Terra-MODIS* images in Figure 2. The superimposed cyan lines show 12-km North American Mesoscale Forecast System (NAM) hybrid-pressure HYSPLIT model (Stein et al., 2015) back trajectories launched from the VMA at 1800 UT (1100 Pacific Daylight Time, PDT). The distributions in Figures 3a and 3d appear similar to the 23 July *Terra-MODIS* image with the Soberanes plume streaming southward over the ocean and the Sand plume drifting northeastward over the Mojave Desert. Figure 3g shows only the Sand Fire emissions rising above 3 km. The low-level HYSPLIT back trajectories in Figures 3a and 3d pass through the San Francisco Bay with the Pacific inflow about 24 hr earlier, while the trajectory at 3.1 km (Figure 3g) follows the northwesterly flow aloft. None of the BBCO tracer had yet reached the SJVAB.

The FLEXPART distributions for 27 July show most of the Soberanes emissions still heading southward along the coast at low altitudes (Figures 3b and 3e), but the smoke is hard to see against the low-lying marine stratocumulus deck in the corresponding *Terra-MODIS* image (Figure 2, middle). The 850 hPa plot in Figure 3e also shows the tracer spreading into the SJVAB toward Fresno at 1.5 km, and the corresponding HYSPLIT back trajectory passes directly over the Soberanes Fire about 48 hr earlier. Figure 3b shows that similar transport also occurred at the 900-hPa level. As before, Figure 3h suggests that the Soberanes plume remained below 3 km on 27 July, but the plot also shows a dispersed BBCO tracer cloud covering the entire SJVAB. Most of this cloud was probably created by lofting of Soberanes smoke, but the 700-hPa back trajectory suggests that some of this tracer may have been emitted by the Sand Fire on the previous day. The low-level winds shifted to the southwest on 30 July and cleared the FLEXPART tracer from the coastal areas. The distributions for 31 July show a more compact Soberanes plume, but the 850-hPa distribution and back trajectory in Figure 3f still suggest that there was significant transport from the Soberanes Fire to the VMA at 1.5 km. Figure 3i shows a smaller tracer cloud at 3 km punctuated by the plume from the Goose Fire. Figure S1 shows the evolution of the FLEXPART BBCO tracer above the Soberanes, Sand, and Goose Fires in addition to the VMA.

4.1. Remote Sensing

The arrival of the Soberanes smoke in the central and southern SJV can be seen in measurements from the NASA-operated AERONET stations at Fresno and Bakersfield (yellow diamonds in Figure 2) (Holben et al., 1998). Figures 4a and 4b show time series of the 340-nm aerosol optical depths (AODs) measured by these stations, which lie about 65 km NW and 110 km SE of Visalia, respectively, during IOP2. These figures also plot the integrated backscatter (IBS) from the TOPAZ lidar, which is roughly proportional to AOD. The time series appear similar, with all three measurements peaking between 27 and 29 July when a distinct haze was visible over the VMA (Figure S2). The two AERONET time series are highly correlated, with a mean Fresno/Bakersfield ratio of 1.05 ± 0.01 ($R = 0.79$). This indicates that most of the smoke became fairly uniformly distributed above the central and southern SJVAB, although the spikiness in late July shows that finer scale plumes were still reaching the eastern valley. Regressions between the Fresno and Bakersfield AODs and the TOPAZ integrated backscatter imply extinction-to-backscatter ratios of $S = 39.6 \pm 0.6$ sr

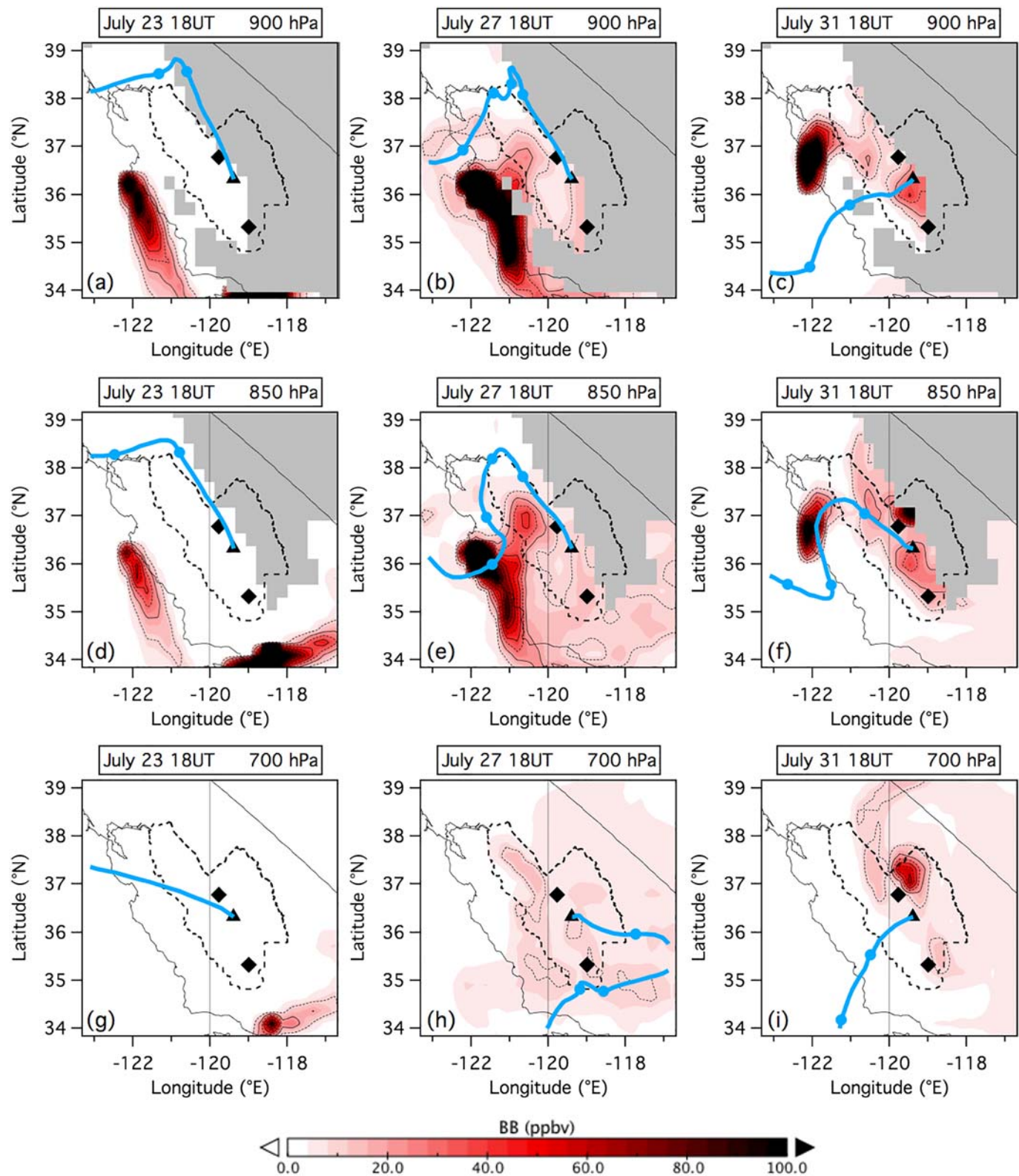


Figure 3. FLEXPART biomass burning CO (BBCO) tracer distributions (red) at 900 hPa (~1 km ASL, a–c), 850 hPa (~1.5 km ASL, d–f), and 700 hPa (~3.1 km ASL, g–i) at 18 UT (11 PDT) on 23, 27, and 31 July. Note that 900 hPa is the lowest calculated level. The cyan lines show 12-km NAM HYSPLIT back trajectories launched from the VMA at 18 UT, and the filled circles mark 12-hr intervals. The black triangles represent the VMA and the filled black diamonds the Fresno and Bakersfield AERONET sites. The dashed black curve outlines the SJVAB. Gray areas represent terrain higher than the pressure level.

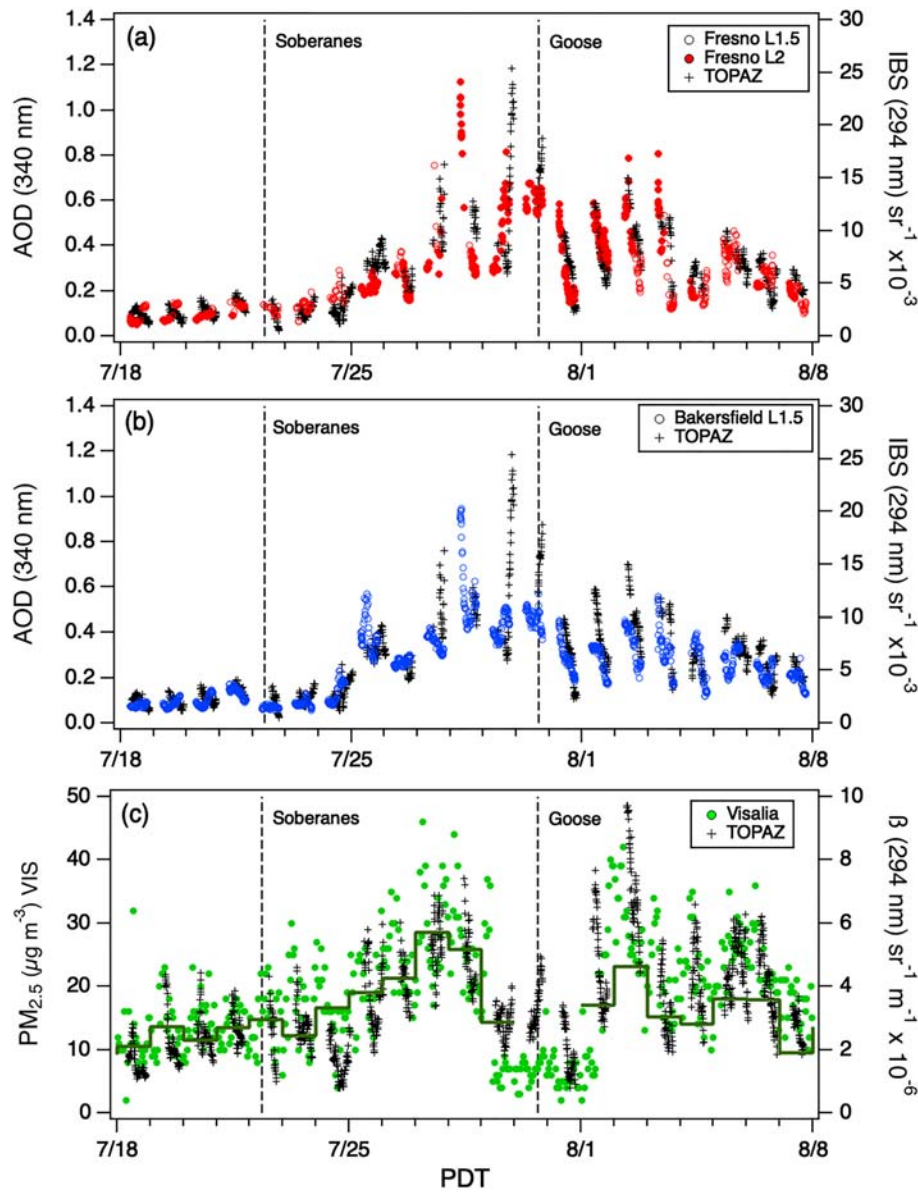


Figure 4. AERONET 340-nm AOD measurements (left axes) from (a) Fresno and (b) Bakersfield, respectively, plotted along with the TOPAZ (25 to 5,000 m agl) integrated backscatter (black crosses, right axis). The open and closed symbols represent the Version 3, Level 1.5, and Level 2.0 AERONET data, respectively. The 340-nm Level 2.0 Bakersfield data were unavailable. (c) Surface $PM_{2.5}$ from the Visalia-N. Church St. CARB monitoring station and the mean 25- to 500-m TOPAZ backscatter. The solid dark green staircase shows the daily average $PM_{2.5}$ which peaked on 27 July.

($R = 0.77$) and 36.9 ± 0.4 sr ($R = 0.81$), respectively, comparable to the value assumed in the lidar retrievals (Langford et al., 2019).

The AOD first began to increase in both cities on 25 July with the Bakersfield station initially reporting higher values than Fresno. HYSPLIT trajectories (not shown) suggest that is due to smoke recirculated inland from the southbound Soberanes plume, although some smoke from the Sand Fire may also have reached Bakersfield. The AOD decreased dramatically on 31 July when southwesterly synoptic winds disrupted the thermal circulations (cf. Figure 3) but briefly increased again on 1–3 August. The maximum AOD value of ~ 1.1 measured in Fresno on the morning of 28 July is larger than the peak of 0.35 measured by the Ames station on 26 July but about 200 times smaller than the AOD of ~ 6 measured only 15 km from the fire by the Monterey AERONET station.

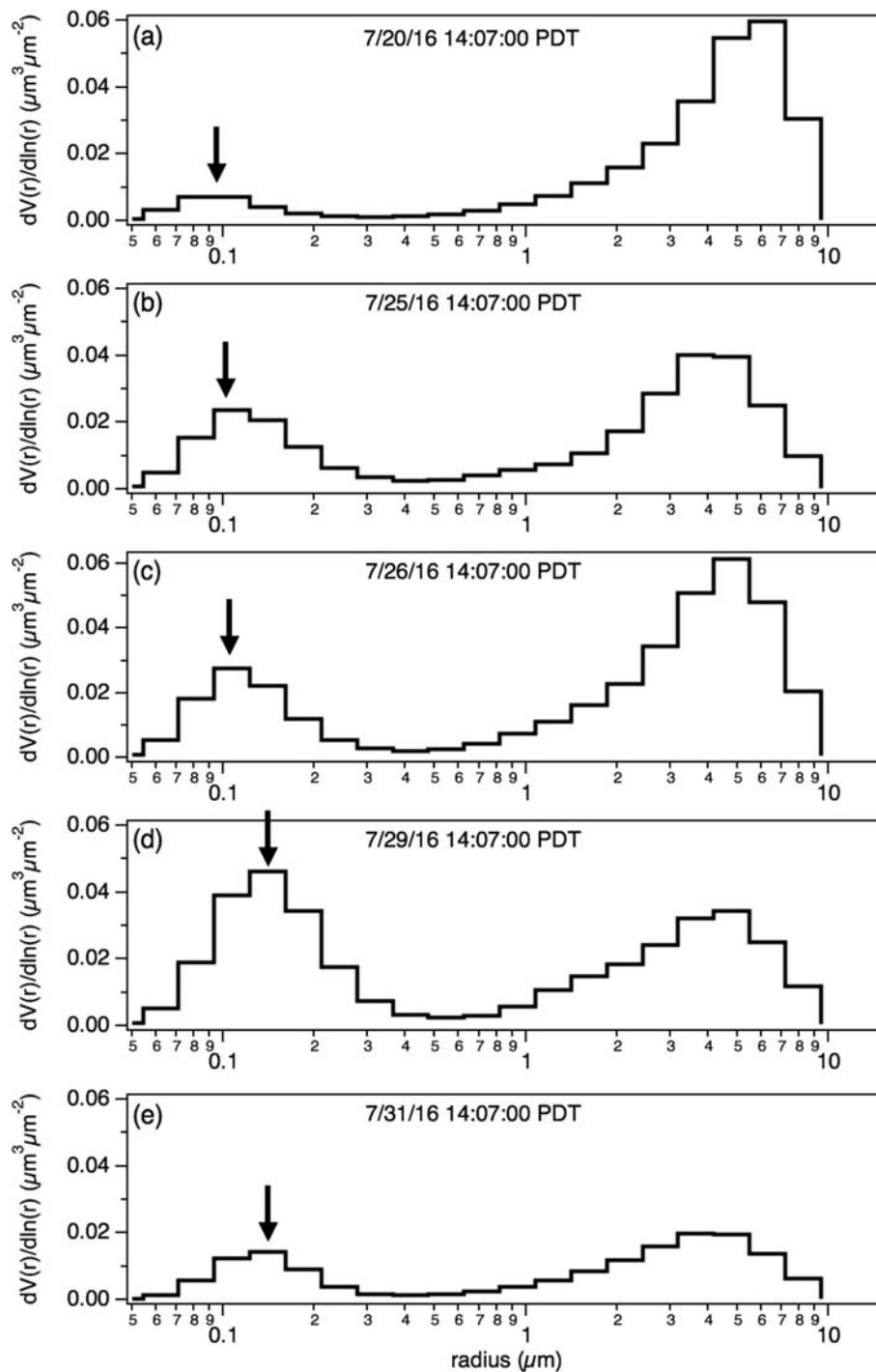


Figure 5. Time evolution of the AERONET aerosol normalized size distributions above Fresno derived from midafternoon measurements. The size distributions before the fire in (a) were dominated by coarse particles with a mode of $\sim 6 \mu\text{m}$ associated with transportation and agricultural activities. The smoke haze was composed of much smaller particles with a mode that increased from ~ 0.11 to $0.15 \mu\text{m}$.

The AERONET stations also retrieved normalized particle size distributions from the multiwavelength measurements using the almucantar method (Holben et al., 1998). Before the start of the fire, the aerosol above both stations was dominated by coarse particles (PM_{10}) with a mode of $\sim 6 \mu\text{m}$ associated with transportation and agricultural activities. A much smaller peak between 0.07 and $0.12 \mu\text{m}$ attributed to photochemistry was also present (Figure 5). After the fire started, the fine particle fraction increased dramatically, with the mode

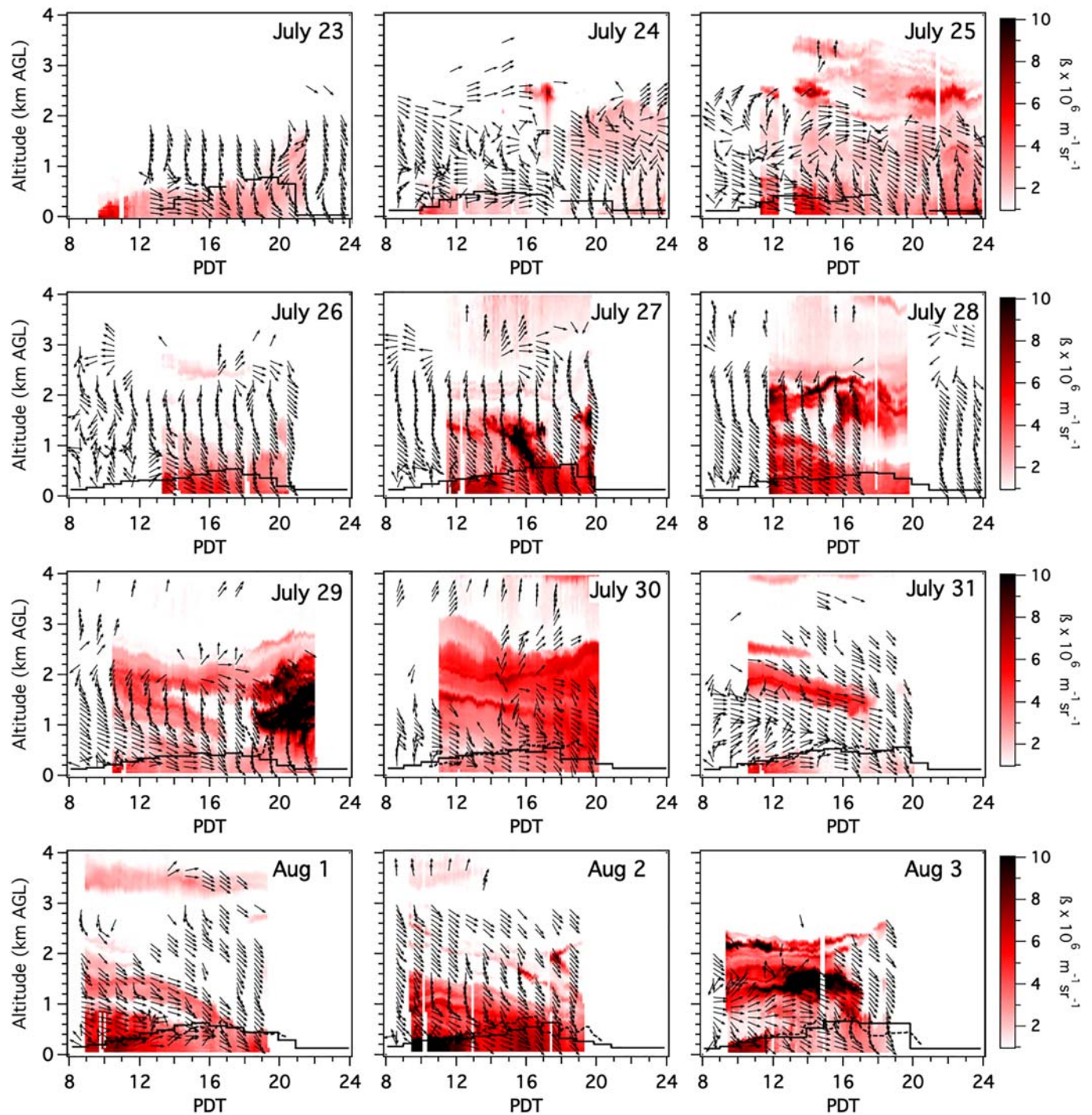


Figure 6. Daily time-height curtain plots of the TOPAZ 294-nm backscatter coefficients (β) measured from 24 July to 1 August. The arrows show the horizontal winds from the 915 MHz profiler, and the black curves the boundary layer heights inferred from the RASS temperature profiles (solid) and vertically staring Doppler lidar measurements (dotted, 30 July to 3 August only) (Bonin et al., 2018). Arrows pointing down and to the right correspond to northwesterly winds.

increasing from $\sim 0.11 \mu\text{m}$ on 25 July to $0.15 \mu\text{m}$ on 29 July, as smoke consisting of black carbon and secondary organic aerosol particles (Park et al., 2007) with ages ranging from ~ 1 day to 1 week accumulated above the SJVAB. These distributions are consistent with previous studies of smoke particle formation and aging (Reid et al., 2005).

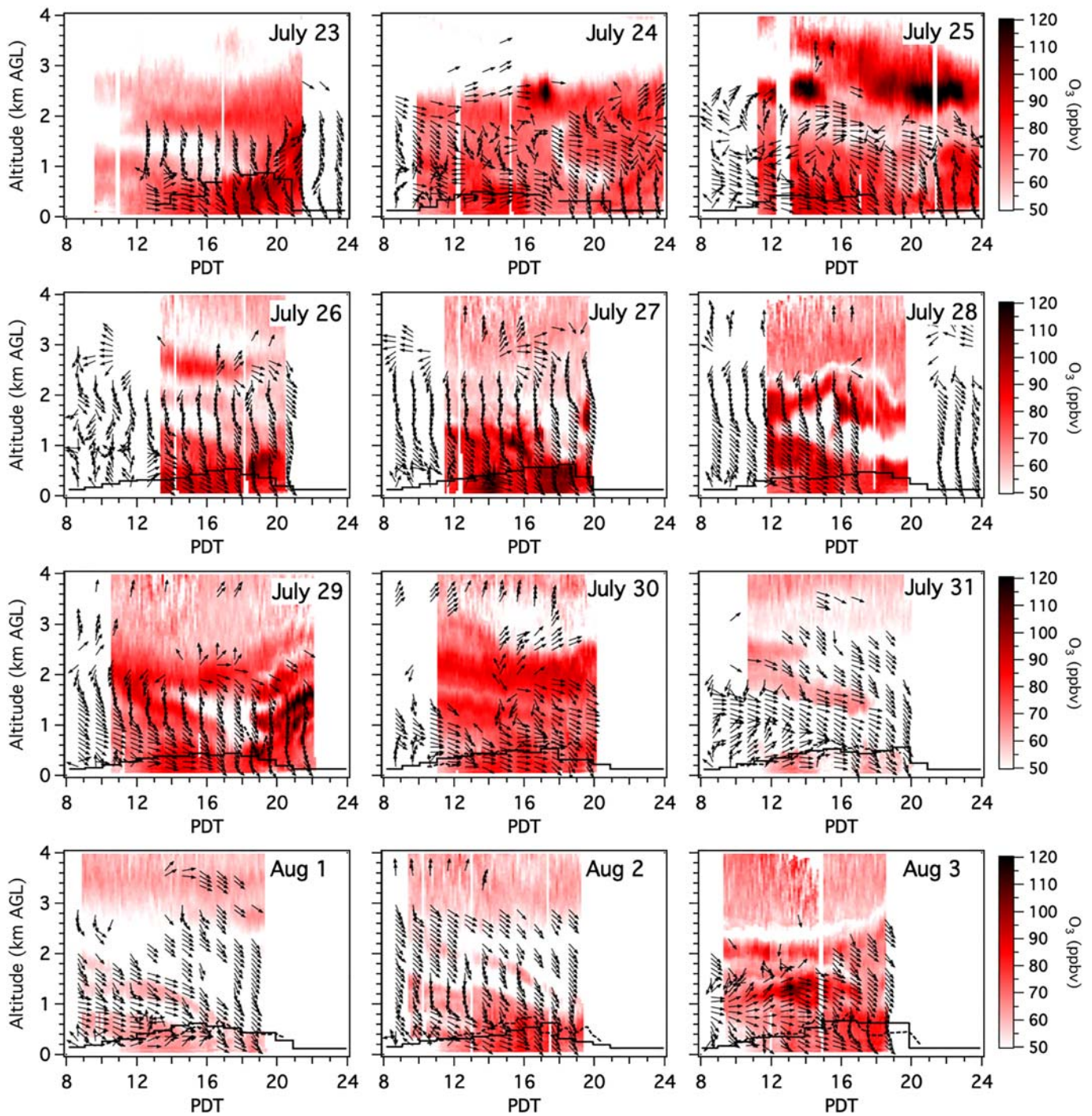


Figure 7. Same as Figure 6 but showing the corresponding TOPAZ O₃ mixing ratios. The highest O₃ (~120 ppbv) was measured around 2.5 km agl on 25 July.

Figure 4c compares the mean TOPAZ backscatter measured between the surface and 500 m and the hourly PM_{2.5} measured by the California Air Resources Board Visalia-N. Church St. monitor 8.5 km east of the VMA in downtown Visalia. These measurements are well correlated ($R = 0.68$ between 13 and 17 PDT when the boundary layer was well mixed) with both time series peaking on 27 July and 2 August. This comparison confirms that the low elevation TOPAZ backscatter is a good proxy for surface PM_{2.5} loadings. The highest daily average PM_{2.5} recorded by the Visalia monitor during CABOTS (29 $\mu\text{g}/\text{m}^3$ on 27 July) remained well

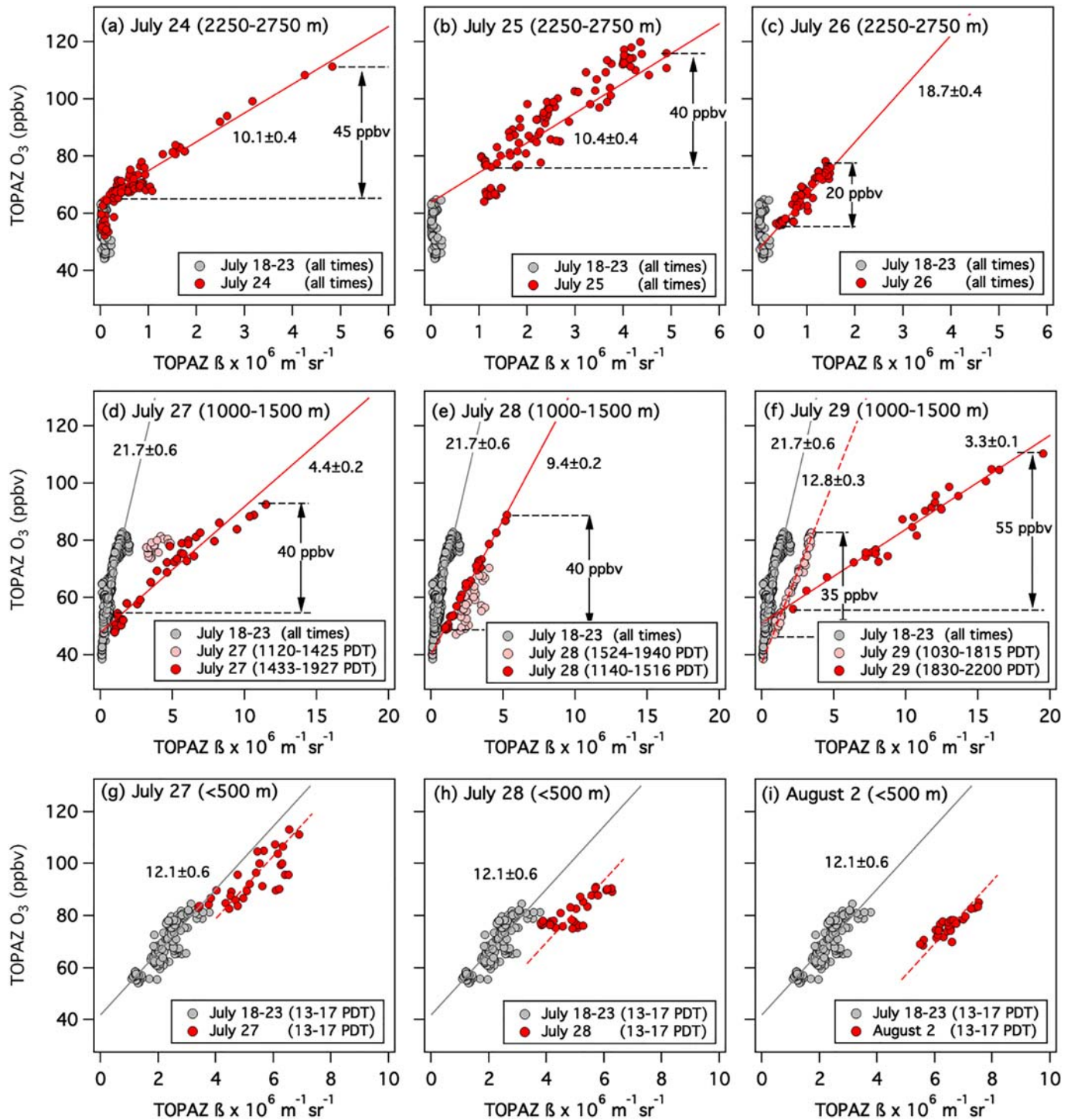


Figure 8. Scatter plots comparing the TOPAZ O_3 and β measurements averaged between 2,250 and 2,750 m on (a) 24 July, (b) 25 July, and (c) 26 July; between 1,000 and 1,500 m on (d) 27 July, (e) 28 July, and (f) 29 July; and between 25 and 500 m on (g) 27 July, (h) 28 July, and (i) 2 August. Note the different horizontal scales. The solid lines in (a)–(f) represent orthogonal distance regression (ODR) fits of the measurements on the indicated days or time intervals; the $\Delta O_3/\Delta\beta$ ratios (in units of 10^6 ppbv $m^{-1} sr^{-1}$) derived from the slopes are shown. The long gray and displaced short dashed red lines in (g)–(i) show fits from the pre-Soberanes (18–23 July) measurements.

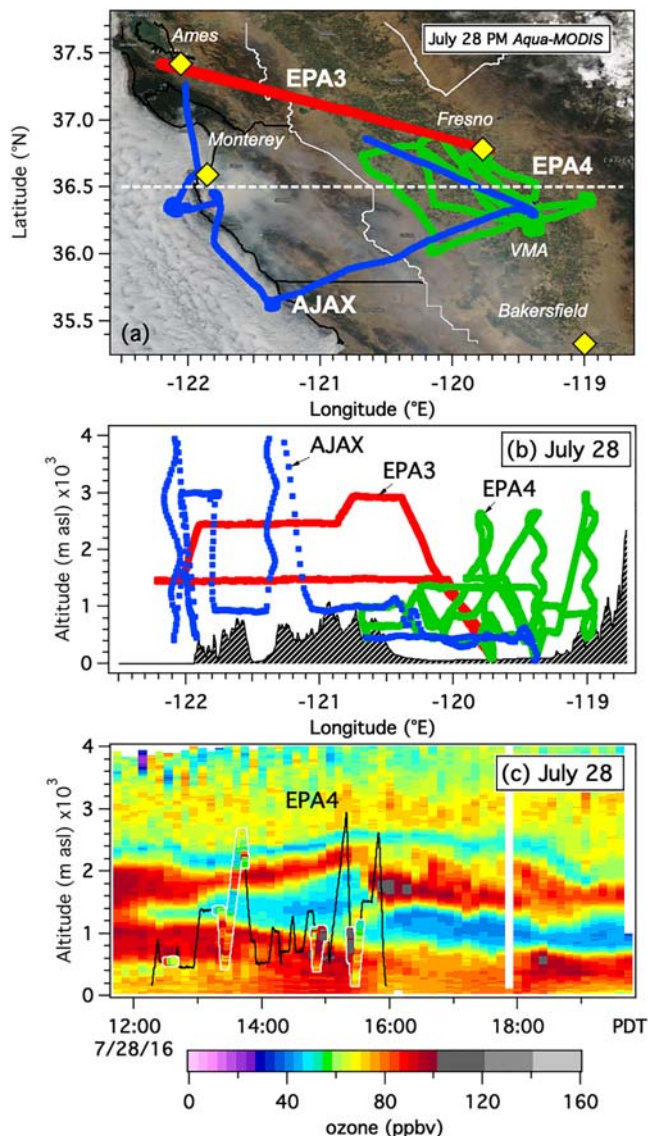


Figure 9. (a) Scientific Aviation morning (EPA3, red) and afternoon (EPA4, green) and AJAX (blue) flight tracks from 28 July superimposed on the afternoon (1330 PDT) Aqua-MODIS image. The yellow diamonds mark the AERONET stations. (b) Altitude-longitude plot of the 28 July flight tracks. The terrain profile corresponds to the dashed white line in (a). (c) Time-height curtain plot of the TOPAZ O₃ measurements from 28 July with the EPA4 flight track superimposed (black). Aircraft measurements made with 15 km of the VMA are colorized to reflect the measured O₃ mixing ratios.

sphere, buffer layer, and mixed layer, respectively. The upper panels show measurements from 24–26 July when the smoke first appeared around 2.5 km, and the middle panels show the measurements from 27–29 July when the AOD and integrated backscatter were highest (cf. Figure 4a). The lower panels show the measurements from 27 July, 28 July, and 2 August when the mixed layer backscatter and Visalia PM_{2.5} loadings were highest (Figure 4c). The gray points in each plot show the measurements made on the 6 days (18–23 June) immediately preceding the appearance of the smoke plume above the VMA.

The 2.5 ± 0.25 -km free tropospheric measurements in Figures 8a–8c show very little aerosol in the free troposphere before the start of the fire and no correlation between this background aerosol and O₃. The mean pre-Soberanes O₃ mixing ratio was 56 ± 5 ppbv, and the mean backscatter was $0.01 \pm 0.09 \times 10^{-6} \text{ m}^{-1} \text{ sr}^{-1}$.

below the NAAQS ($35 \mu\text{g}/\text{m}^3$) showing that the Soberanes Fire did not severely impact the particulate air quality in the Visalia area.

The vertical distribution of the smoke above the VMA is shown in Figure 6, which displays daily time-height curtain plots of the TOPAZ backscatter measured between 23 July and 3 August. These plots also show the horizontal winds measured by the colocated 915-MHz radar profiler and the boundary layer heights inferred from the Radio Acoustic Sounding System temperature measurements. The wind patterns on most of the measurement days appear similar to the measured and WRF-simulated winds for 29 July to 3 August 2000 from the Central California Ozone Study shown in Bao et al. (2008). The winds in the lowest 2 km were generally up-valley (north northwesterly) due to the strong inflow through the San Francisco Bay, but a strong westerly component appears in the lowest 1 km during the day as upslope flow into the Sierra Nevada develops. The low-level winds then accelerate and rotate to the northwest around 1700 PDT (0000 UT) as a low-level jet develops during the night (Bao et al., 2008).

The top middle panel of Figure 6 shows the first smoke appearing from the west at about 2.5 km at 1700 PDT on the afternoon of 24 July. More diffuse smoke followed between 1 and 2 km later that evening, and enhanced backscatter was measured from the surface to about 3.5 km on 25 July with several pockets of denser smoke appearing around 2.5 km. The backscatter aloft briefly decreased on 26 July when the winds above 1 km became more northerly but increased again the following day and remained high through 30 July. The densest backscatter was measured between 1 and 2 km on the evening of 29 July with denser smoke also appearing at these altitudes on 27 July and 3 August. Backscatter diminished at most altitudes on 31 July when the winds above the boundary layer became southwesterly but began to increase again the next day, recovering first in the boundary layer and then in the buffer layer as the thermal circulations reestablished (cf. Figure 4c). The narrow tongue appearing around 2 km on 31 July is likely due to the nearby Goose Fire. Light smoke from this fire was still present between 3 and 4 km on 1 and 2 August.

5. Ozone Production in the Smoke Plume

The time-height curtain plots in Figure 7 are analogous to those in Figure 6 but instead show the O₃ mixing ratios measured by the TOPAZ lidar. The striking similarities between these two figures show at a glance that substantial O₃ was formed in the Soberanes Fire plume. The correlation between ozone and backscatter is more obvious in Figure 8, which displays scatter plots of the mean O₃ and β measured within 2.5 ± 0.25 , 1.25 ± 0.25 , and 0.25 ± 0.25 km altitude bins representing the free tropo-

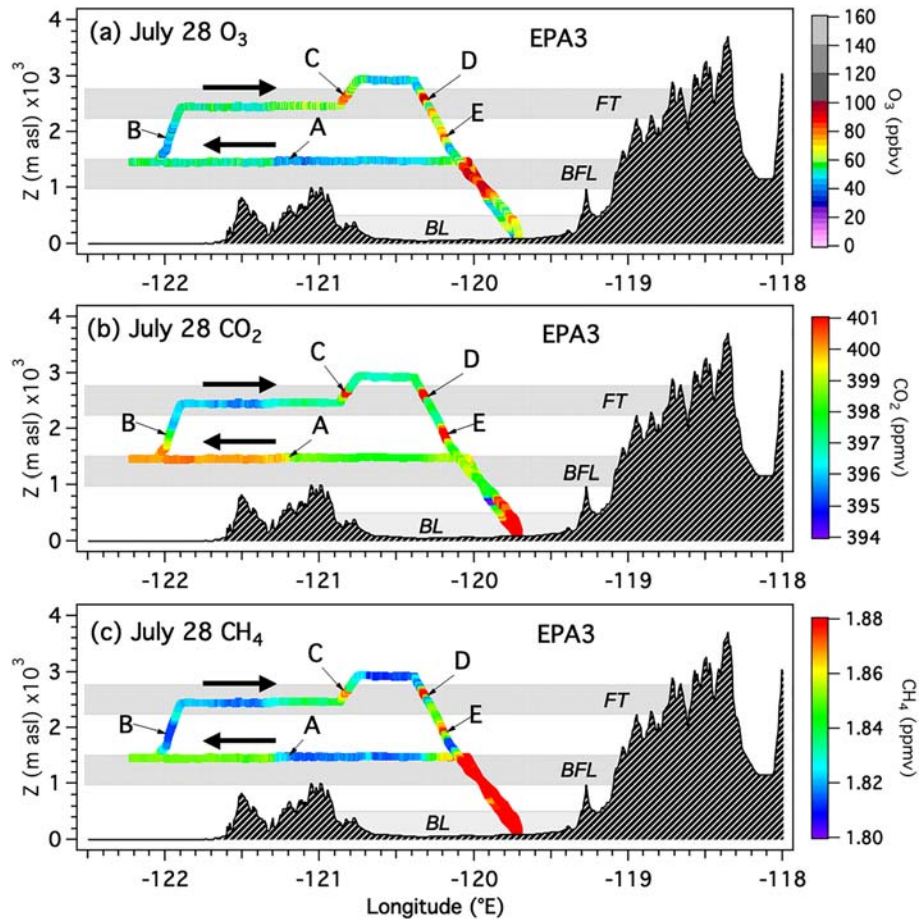


Figure 10. Altitude-longitude plots showing the flight tracks from the TLS morning (EPA3, 0757–0952 PDT) flight on 28 July colored by the measured: (a) O_3 , (b) CO_2 , and (c) CH_4 concentrations. The background terrain corresponds to the dashed transect south of Fresno in Figure 9a. The labels (A–E) are described in the text. The gray bands show the “boundary layer” (BL), “buffer layer” (BFL), and free troposphere (FT) altitude ranges used in Figure 8. The morning flights on 27 July (EPA1) and 29 July (EPA5) followed similar flight tracks.

Both O_3 and β increased dramatically when the first smoke appeared from the west on the afternoon of 24 July, however, with the measured O_3 mixing ratios climbing to more than 110 ppbv. The measurements from 25 July show up to 120 ppbv of O_3 , but both O_3 and β decreased on 26 July after the winds shifted to the north (cf. Figures 4 and 6). These plots are analogous to the $\Delta O_3/\Delta CO$ or $\Delta O_3/\Delta CO_2$ mixing/dilution plots used in many studies where CO (e.g., Jaffe & Wigder, 2012) or CO_2 (Yates et al., 2016) is used as the passive tracer. The linearity of the O_3 - β relationships in these plots suggests that the lidar backscatter can also be used as a tracer and implies that (i) most of the O_3 production occurred in the 24–48 hr before the smoke reached the VMA, (ii) the background O_3 concentrations were relatively constant over the sampling periods shown in these plots, and (iii) the observed variations were controlled primarily by mixing between the advected fire plume and the surrounding free tropospheric air. The differences between the highest and lowest O_3 concentrations along the mixing lines give lower limits for the amount of O_3 produced in the plume, with ≥ 45 ppbv of excess O_3 measured on 24 July (Figure 8a).

Figures 6 and 7 show that the backscatter and O_3 in the buffer layer (1.25 ± 0.25 km) increased significantly on 27 July after the winds aloft shifted from westerly to northerly on 26 July. Figure 3b shows that the corresponding HYSPLIT trajectories arrived from northerly but passed over the Soberanes Fire about 48 hr earlier. The densest smoke and highest O_3 were measured on the evening of 29 June (Figure S2). The scatter plots in Figures 8d–8f show strong linear correlations between O_3 and β , but the interpretation of these measurements is complicated by the presence of anthropogenic O_3 and particulates from the boundary layer. These

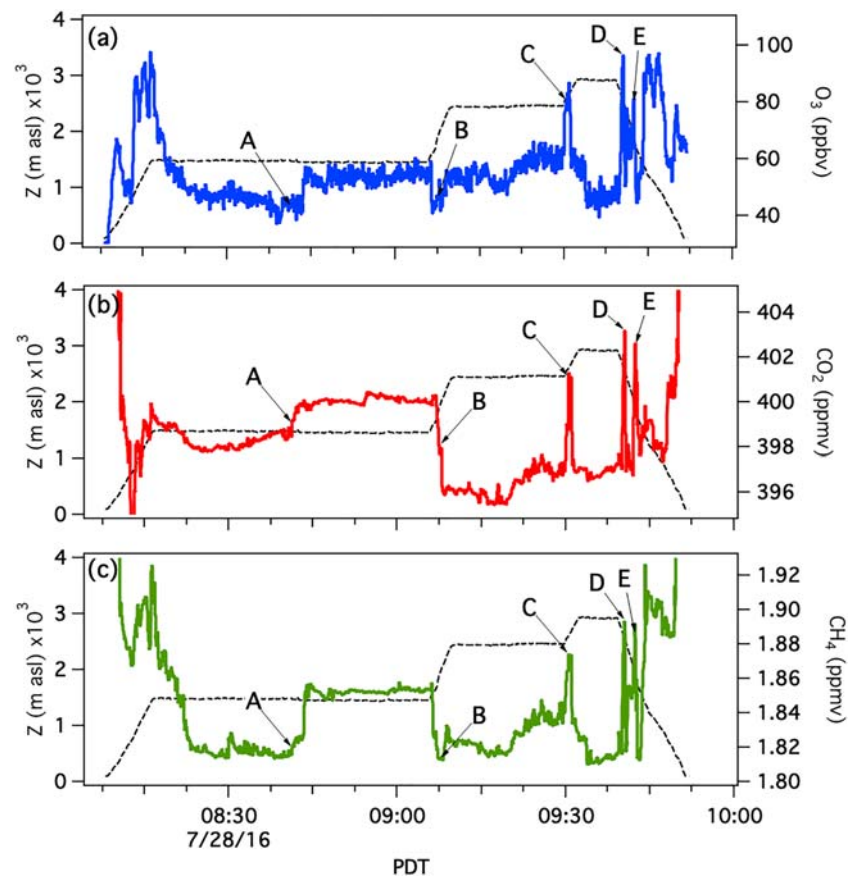


Figure 11. Time series of the (a) O_3 , (b) CO_2 , and (c) CH_4 measured on the morning flight from Fresno to San José and back on 28 July (EPA3). The locations corresponding to the labels A–E are show in Figure 10. The dashed black lines represent the flight altitude.

anthropogenic contributions caused the O_3 mixing ratios in the buffer layer to exceed the corresponding free tropospheric values by more than 30 ppbv on both 20 and 21 June, and the mean pre-Soberanes O_3 mixing ratio of 62 ± 10 ppbv was 5.5 ppbv greater than the free tropospheric value. The mean pre-Soberanes backscatter was also higher in the buffer layer ($0.6 \pm 0.4 \times 10^{-6} \text{ m}^{-1} \text{ sr}^{-1}$). The orthogonal distance regression (ODR) fits in Figures 8d–8f have intercepts between 40 and 50 ppbv, which are comparable to the mean value of 43 ± 2 ppbv of O_3 measured by Scientific Aviation (see below) upwind of the fire at 1.45 km asl on the morning of 29 July. Figure 8f shows that the difference between the highest (111 ppbv) and lowest (56 ppbv) concentrations measured on the evening of 29 July was 55 ppbv, but some of this O_3 may have originated from anthropogenic sources.

The ODR fits in Figures 8a–8f vary widely, but Figure S3 shows that the $\Delta O_3/\Delta\beta$ ratios in the buffer layer and free troposphere decreased exponentially with increasing peak backscatter. A recent analysis of surface measurements by Buysse et al. (2019) also found less O_3 production in some denser smoke plumes. Possible reasons for the decrease in Figure S3 include reduced actinic fluxes in the denser smoke plumes, O_3 losses on aerosol surfaces, or changes in the fuels and/or combustion regime. A higher $\Delta O_3/\Delta\beta$ ratio might be expected for flaming combustion which usually produces more NO_x and less smoke than smoldering combustion (Yokelson et al., 2008). It could also be argued that O_3 is still being formed in the denser smoke plumes, which are presumably younger than the more dispersed smoke, but this explanation seems inconsistent with the linearity of the scatter plots, which is more easily explained by mixing.

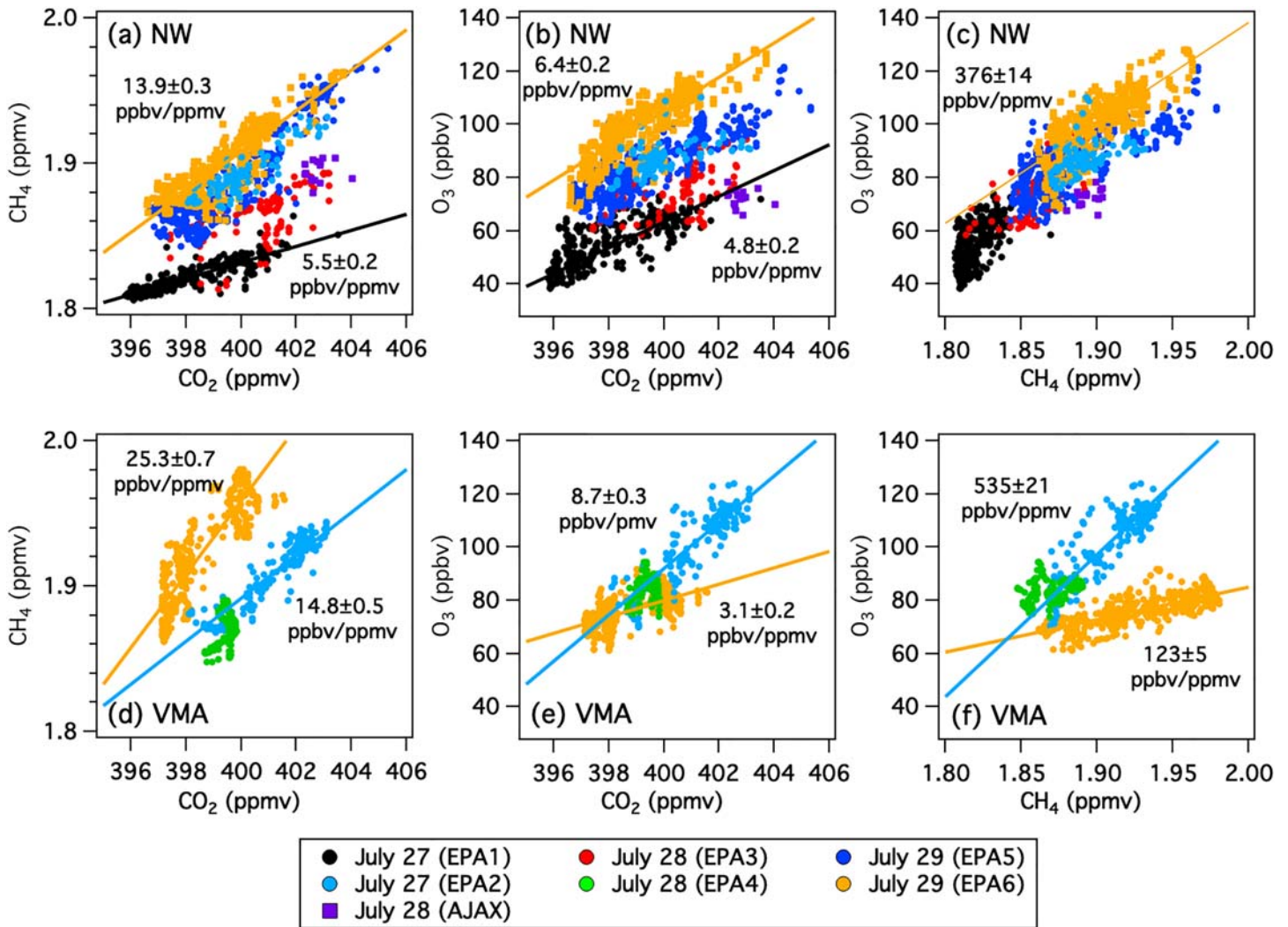


Figure 12. Scatter plots comparing: (a) CH₄ and CO₂, (b) O₃ and CO₂, and (c) O₃ and CH₄ concentrations measured between ~1.5 and 2.5 km asl by the TLS and AJAX aircraft. The top panels show measurements from discrete smoke plumes sampled over the northwestern SJVAB and coast ranges. The bottom panels (d–f) show measurements made within 20 km of the VMA. The colored lines show orthogonal distance regression (ODR) fits of the plotted data.

Figures 8g–8i show the backscatter and ozone measured near the surface. Only measurements made between 13 and 17 PDT, when the boundary layer was well mixed and at least 500 m deep, are shown. These plots also show that there was much less smoke near the surface than in the buffer layer, with the largest afternoon backscatter enhancement measured on 2 August (cf. Figures 4c). The measurements from 27 July (Figure 8g) show much higher O₃ mixing ratios than were measured in the 6 days before the fire but lie slightly below and very close to the pre-Soberanes mixing line. This suggests that either the high O₃ (~110 ppbv) measured on that day was man made or that the O₃ production rate (relative to PM) in the smoke was similar to that of the anthropogenic pollution. The measurements from 28 July and 2 August (Figures 8h and 8i) also follow the same slope as the pre-Soberanes measurements but are significantly displaced from the mixing line. The O₃ mixing ratios are slightly higher than those measured before the fire, but these displacements can also be explained without any invoking any fire-related O₃ enhancements (cf. section 6). The differences between the buffer layer and mixed layer measurements suggest that the surface smoke was transported up the valley with the Pacific inflow and not mixed downward from the buffer layer. We note that the buffer layer-boundary layer coupling may have been stronger in the southern SJV where the subsidence is stronger and vertical mixing by the nocturnal low-level jet important (Caputi et al., 2019).

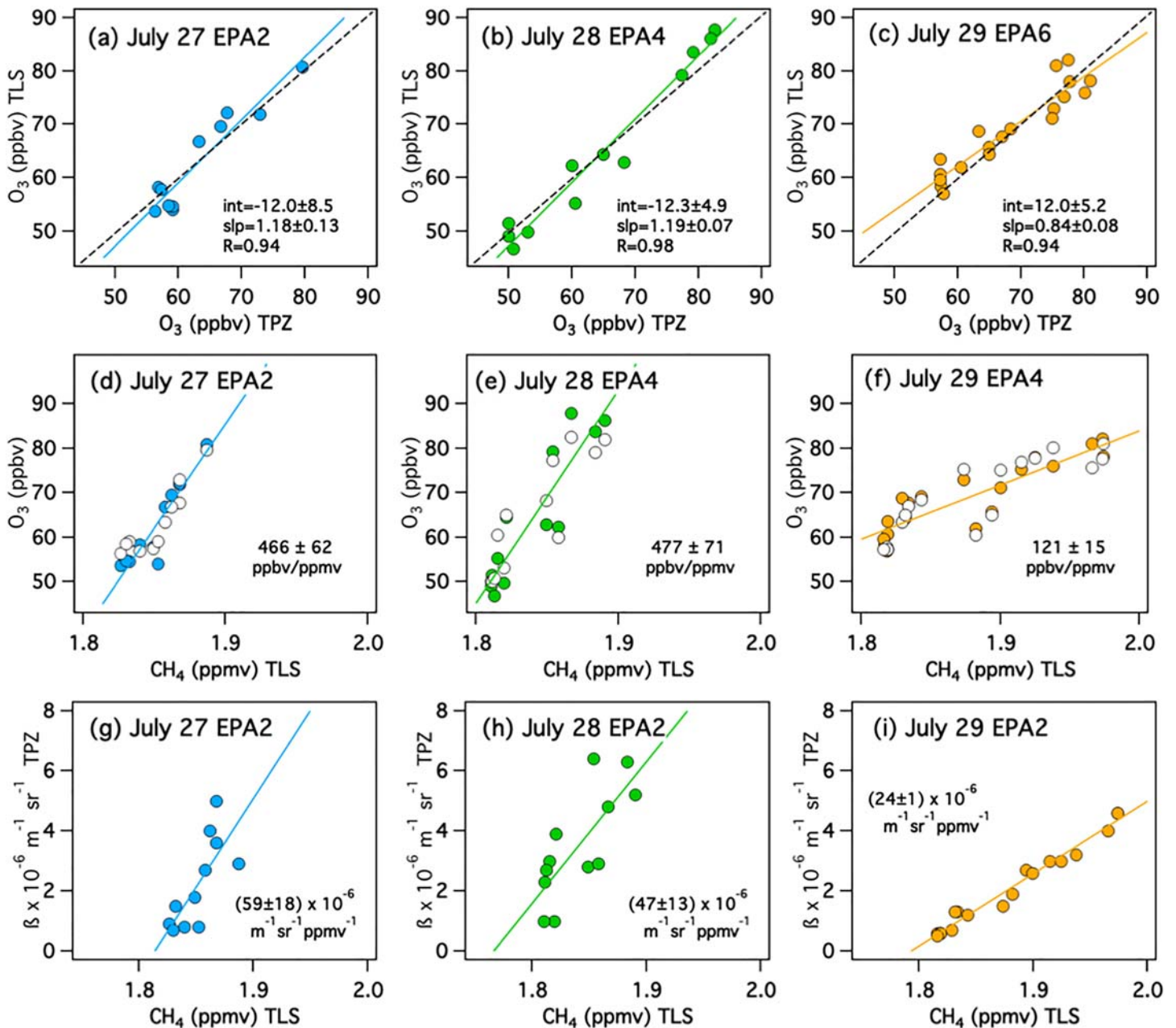
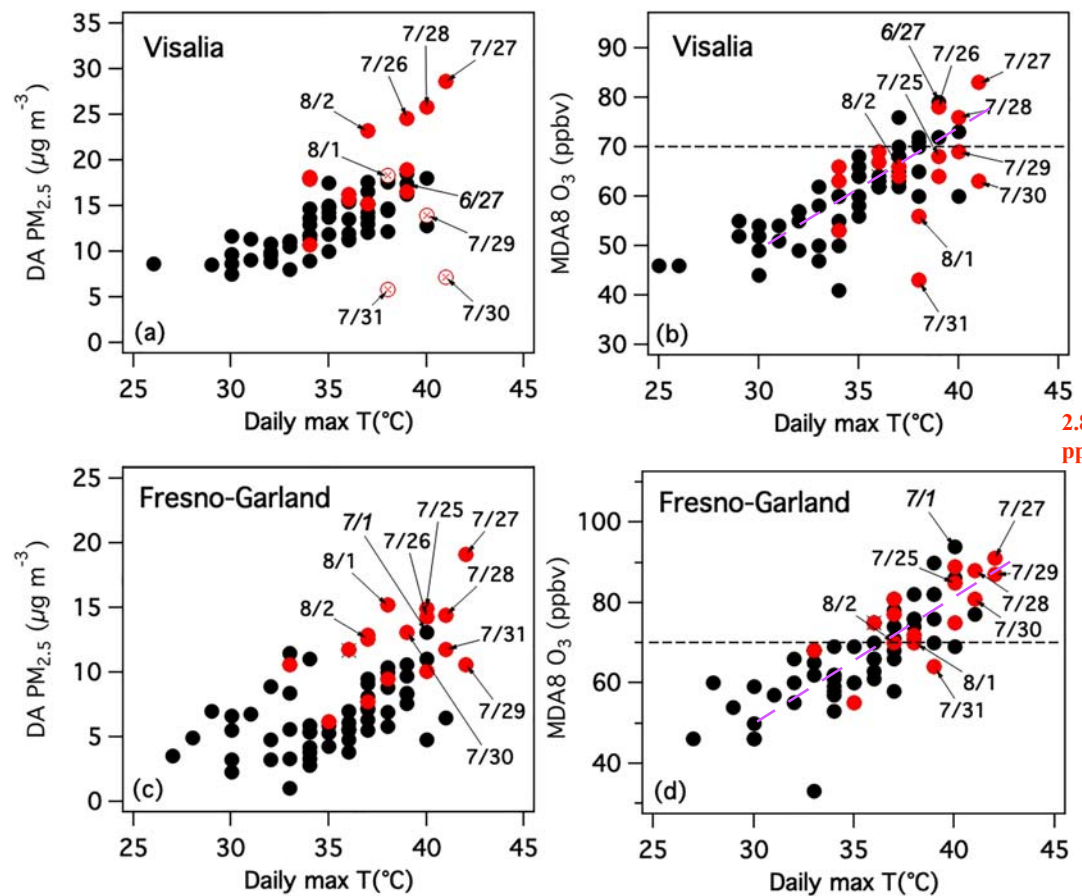


Figure 13. Scatter plots comparing the retrieved O_3 and β from the TOPAZ profiles to TLS in situ CH_4 measurements made within 20 km of the lidar on EPA2 (1327–1338 PDT), EPA4 (28 July, 1326–1342 PDT), and EPA6 (29 July, 1449–1505 PDT). Panels (a)–(c) compare the TOPAZ O_3 and TLS O_3 measurements. The dashed lines show the 1:1 correspondence. Panels (d)–(f) compare the TLS (filled circles) and TOPAZ (open circles) O_3 measurements to the TLS CH_4 . Panels (g)–(i) compare the TOPAZ β to the TLS CH_4 . The solid lines in all of the plots show orthogonal distance regression (ODR) fits to the plotted data. See Figure 12 for the color scheme.

5.1. Aircraft Measurements

The Soberanes smoke was sampled by the Scientific Aviation Mooney TLS Bravo research aircraft (<http://www.scientificaviation.com>) on 27–29 July (TLS) during flights supported by the U.S. EPA and the Bay Area Air Quality Management District. Additional flights were conducted on 4–6 August but will not be discussed here. The TLS carried a 2B Technologies Model 205 O_3 monitor and a Picarro 2301f Cavity Ring-Down Spectrometer to measure CO_2 , CH_4 , and H_2O . The aircraft also carried an Eco Physics Model CLD 88 chemiluminescence detector with a photolytic converter for NO_2 , but these measurements were plagued by noise on some of the flights (Trousseau et al., 2019) and are not used here. The ad hoc



2.8 & 3
ppb/K

Figure 14. Scatter plots showing the (a) daily average $PM_{2.5}$ and (b) MDA8 O_3 from the Visalia N. Church St. monitor as a function of daily maximum temperature during all of CABOTS. Panels (c) and (d) show the corresponding measurements from the Fresno-Garland monitor colocated with the AERONET. Note the different vertical scales. The black points show measurements made before the Soberanes Fire started (27 May to 22 July) and the red points those made after the fire started (23 July to 7 August). The partially filled circles in (a) are from days when only preliminary $PM_{2.5}$ data were reported at Visalia. The horizontal dashed lines in (b) and (d) show the 70 ppbv NAAQS.

EPA/Bay Area Air Quality Management District program consisted of morning (0800–1000 PDT) flights between Fresno and San José and afternoon (1200–1600 PDT) flights above the Fresno-Visalia area. In the following discussion, odd numbers refer to the morning flights (EPA1, EPA3, and EPA5) and even numbers the afternoon flights (EPA2, EPA4, and EPA6). The afternoon flights included low approaches and/or spiral profiles at the VMA for comparisons with TOPAZ and the in situ surface measurements at the VMA. The aircraft, lidar, and in situ measurements of O_3 agreed to within ± 5 ppbv on average during these comparisons (Langford et al., 2019).

The Soberanes emissions were also sampled by the NASA Alpha Jet Atmospheric eXperiment (AJAX) (Yates et al., 2016) during an afternoon flight on 28 July. The Alpha Jet carried an external wing pod with a modified commercial ultraviolet absorption monitor (2B Technologies Inc., model 205) to measure O_3 (Ryoo et al., 2017; Yates et al., 2015; Yates et al., 2013) and a (Picarro model 2301-m) cavity ring-down analyzer to measure CO_2 , CH_4 , and H_2O (Tanaka et al., 2016). A second wing pod carried a nonresonant laser-induced fluorescence instrument to measure formaldehyde (CH_2O) (St. Clair et al., 2017). The AJAX O_3 measurements were also compared with TOPAZ during profiles and low approaches at the VMA before the start of the Soberanes Fire, and these comparisons likewise found agreement to within ± 5 ppbv (Langford et al., 2019). AJAX also sampled the Soberanes plume on several flights conducted after the end of the CABOTS campaign that will not be discussed here. Unfortunately, neither aircraft measured particulates or CO since wildfires were not the primary focus of the CABOTS campaign.

Figure 9a shows flight tracks from the two 28 July TLS sorties (EPA3: 0808–0952 PDT and EPA4: 1212–1558 PDT) and the 28 July AJAX (1426–1602 PDT) flight, superimposed on the (1330 PDT) *Aqua-MODIS* image. The winds were relatively calm on 28 July, and the *Aqua-MODIS* image shows diffuse smoke haze covering the Coast Ranges and south central SJVAB with fresher smoke lingering near the fire. Figure 9b shows the same flights as altitude-longitude plots, and Figure 9c is a time-height curtain plot of the 28 July TOPAZ O₃ measurements with the EPA4 flight track superimposed (black line). The portions of the track within 20 km of the VMA are colorized to show the O₃ concentrations measured by the aircraft. These measurements show the excellent agreement between the two techniques.

Figure 10 shows the O₃, CO₂, and CH₄ measurements from EPA3 (28 July) as colorized altitude-longitude plots. The gray bands show the “boundary layer,” “buffer layer,” and “free troposphere” altitude bins used in Figure 8. These plots show that the CO₂ concentrations fell quickly as the TLS climbed out of the shallow boundary layer near Fresno, but the CH₄ concentrations remained high through the top of the buffer layer. Figure 10a shows that O₃ was elevated in the buffer layer with much lower concentrations in the boundary layer. The late morning TOPAZ O₃ measurements show a similar structure. The TLS cruised northwestward at about 1.4 km asl and entered a broad plume with elevated CO₂, CH₄, and O₃ about 80 km north of the fire at Point A. The aircraft climbed out of this plume at about 1.9 km asl (Point B) as it ascended to 2.5 km for the return leg to Fresno. It passed through a thin layer with much higher CO₂, CH₄, and O₃ around 2.6 km asl (Points C and D) on the return leg and descended through a second, similar layer at 1.9 km asl (Point E) during the approach to Fresno. The O₃, CO₂, and CH₄ measurements from EPA3 are plotted as time series in Figure 11. The O₃ enhancements in some of the narrow peaks exceed 50 ppbv.

5.2. Emission Ratios

Since neither aircraft measured CO, we calculate methane emission ratios (MER) relative to CO₂, and ozone production rates (OPR) relative to both CO₂ and CH₄. Both compounds are emitted by biomass burning, but their usefulness as reference tracers is compromised in the boundary and buffer layers since CO₂ is taken up by growing vegetation, and there are large agricultural and petrochemical sources of CH₄ in the SJVAB (Peischl et al., 2018; Peischl et al., 2012; Trousdell et al., 2016). In the following discussions, we therefore restrict our analyses of the aircraft data to measurements made above 1.5 km. For these calculations, we create scatter plots from the 1-s measurements acquired during the roughly 1 min required for the aircraft to fly through one of the narrow plumes corresponding to the labeled peaks in Figure 11 and similar time series from the other EPA and AJAX flights.

Figure 12a shows that the CH₄ and CO₂ measurements from EPA1 (black points) fall on a straight line with a well-defined intercept consistent with the mixing of a fine-scale plume into air with constant background concentrations (Yokelson et al., 2013). An orthogonal linear regression fit of these points gives a MER of 5.5 ± 0.2 ppb CH₄ (ppm CO₂)⁻¹. The measurements from EPA6 (orange points) follow a much steeper line corresponding to 13.9 ± 0.3 ppb CH₄ (ppm CO₂)⁻¹. Fits are not shown for the measurements from the other flights, which fall between these two extremes with the measurements from different parts of some flights (e.g., EPA3, red points) following more than one mixing line.

MERs are not usually reported relative to CO₂ if CO measurements are available, but the values derived here are similar to those derived from AJAX measurements (Yates et al., 2016) near Yosemite National Park made during the 104,058 ha (257,134 acre) Rim Fire as part of the 2013 SEAC⁴RS (Studies of Emissions, Atmospheric Composition, Clouds and Climate Coupling by Regional Surveys) campaign (Toon et al., 2016). The Rim Fire burned in brush, oak, and pine stands located at higher elevations than the Soberanes Fire, but analysis of smoke plumes sampled by AJAX on 26 and 29 August, 2013, when the Rim Fire was still actively expanding, yielded MERs of 8.0 and 6.5 ppb CH₄ (ppm CO₂)⁻¹, comparable to the value shown in Figure 12a from the EPA1 (27 July) measurements. AJAX measurements made 2 weeks later when the Rim Fire was mostly smoldering yielded a much higher MER of 18.3 ppb CH₄ (ppm CO₂)⁻¹, which is closer to the MER derived from EPA6 (29 July). These values can also be compared to MERs ranging from 7.4 to 22.0 ppb CH₄ (ppm CO₂)⁻¹ inferred from surface measurements of CH₄ and CO₂ during four different wildland fires and prescribed burns in mixed conifer forests of the northern Rocky Mountains (Urbanski, 2013).

The wide range of MERs derived from the data in Figure 12a can be explained by the sampling of emissions from different combustion regimes; higher MERs are associated with smoldering combustion, which usually generates more particulates and reduced compounds (e.g., CO, CH₄, nonmethane organic compounds, and NH₃), while lower MERs are associated with flaming combustion, which typically emits fewer particulates and more fully oxidized species (e.g., CO₂ and NO_x) (Akagi et al., 2011; Urbanski, 2013; Yokelson et al., 2008). The large plume-to-plume variability on some flights was probably caused by the sampling of smoke originating from different parts of the rapidly growing fire.

Figures 12b and 12c are similar to Figure 12a but show the corresponding O₃ mixing ratios plotted as a function of CO₂ and CH₄, respectively. The OPRs taken from the slopes in Figure 12b show less variability than the MERs with values between 4.8 and 6.4 ppbv ppb O₃ (ppm CO₂)⁻¹. OPRs are also rarely reported relative to CO₂, but these values are larger than the OPRs from the Rim Fire measurements of 29 August 2013, which found 2.0 ppb O₃ (ppm CO₂)⁻¹ within the main Rim Fire smoke plume, and 2.7 ppb O₃ (ppm CO₂)⁻¹ within the smoke haze filling a nearby valley. However, the values derived here are closer to the OPR of 7.3 ppb O₃ (ppm CO₂)⁻¹ inferred from the reported ΔO₃/ΔCO and ΔCO/ΔCO₂ emission rates in the 4-hr-old fire plume from a prescribed fire in a similar chaparral ecosystem (primarily scrub oak and sagebrush) near San Luis Obispo California (Akagi et al., 2012). Interestingly, the intercepts in Figure 12b change by nearly a factor of 2 from day to day, but this variability collapses in Figure 12c.

The measurements from the afternoon EPA flights above the valley show even more variability. The TLS executed a profile and/or close approach at the VMA on each of the afternoon EPA flights (i.e., EPA2, EPA4, and EPA6), and the scatter plots in the lower panels of Figure 12 show the in situ measurements (above 1.5 km asl) along those flight segments.

Figure 12d shows that the measurements from EPA2 (27 July, cyan points) fall on a line giving a MER of 14.8 ± 0.5 ppb CH₄ (ppm CO₂)⁻¹, which is similar to the values derived from the measurements made above the coastal mountains on both EPA2 and EPA6 (29 July, orange points). The EPA4 measurements (28 July, green points) near the VMA fall approximately on the same line, but the EPA6 (29 July, orange points) measurements near the VMA give a much larger MER of 25.3 ± 0.7 ppb CH₄ (ppm CO₂)⁻¹. The OPRs calculated from the EPA6 VMA measurements (Figures 12e and 12f, orange points) are also much smaller than those derived from measurements made further west on the same flight and using the same analysis technique, which precludes possible contamination by other CH₄ sources.

Figure 13 compares the TLS measurements from the VMA profiles on the EPA2 (27 July), EPA4 (28 July, cf. Figure 10c), and EPA6 (29 July) flights with the nearest TOPAZ O₃ and β measurements (<20 km). The individual points in these plots represent samples taken between 1,500 and 2,500 m asl at roughly 100- to 200-m intervals and include both buffer layer and free tropospheric samples. The reasonable agreement between the lidar and aircraft O₃ measurements in the top row lends confidence to the assumption that the lidar and aircraft were sampling similar air masses on all 3 days; more rigorous intercomparisons are described elsewhere (Langford et al., 2019). The middle panels (Figures 13d–13f) show that the OPRs (relative to CH₄) estimated from these sparsely sampled measurements are similar to those derived from the more complete plume analyses in Figure 12f. The bottom panels (Figures 13g–13i) also show good correlations between the TOPAZ backscatter and the TLS CH₄, which supports the use of β as biomass burning tracer.

These comparisons between the lidar and aircraft shed no further light on the reason for the smaller slopes in the 29 July measurements in Figures 12f and 13i, but one possible explanation is suggested by HYSPLIT back trajectories (not shown), which indicate that the air sampled about ~1.5 km above the VMA on EPA2 (27 July) passed near the Soberanes Fire about 48 hr earlier, while the air sampled on EPA6 (29 July) spent the previous 72 hr circulating between the SJVAB and the Sierra Nevada, which may have depleted both smoke and O₃ relative to CH₄.

6. Impact on Surface Air Quality in the SJVAB

The arrival of the Soberanes smoke plume coincided with the highest surface O₃ measured in the SJVAB during 2016. The two highest recorded 1-hr O₃ concentrations (120 and 131 ppbv) of the year were measured midway between Fresno and Visalia at Parlier on 27 and 29 July, respectively, and the highest MDA8 (101 ppbv) was recorded at Parlier on 27 July. The Visalia monitor also reported its highest MDA8 value

Acknowledgments

The California Baseline Ozone Transport Study (CABOTS) field measurements were funded by the California Air Resources Board (CARB) under Contracts 15RD012 (NOAA ESRL), 14-308 (UC Davis), and 17RD004 (NASA Ames). We would like to thank Jin Xu and Eileen McCauley of CARB for their support and assistance in the planning and execution of the project and are grateful to the CARB and the San Joaquin Valley Air Pollution Control District (SJVAPCD) personnel who provided logistical support during the execution of the field campaign. We would also like to thank Cathy Burgdorf-Rasco of NOAA ESRL and CIRES for maintaining the CABOTS data site. The NOAA team would also like to thank Ann Weickmann, Scott Sandberg, and Richard Marchbanks for their assistance during the field campaign. The NOAA/ESRL lidar operations were also supported by the NOAA Climate Program Office, Atmospheric Chemistry, Carbon Cycle, and Climate (AC4) Program and the NASA-sponsored Tropospheric Ozone Lidar Network (TOLNet, <http://www-air.larc.nasa.gov/missions/TOLNet/>). The UC Davis/Scientific Aviation measurements were also supported by the U.S. Environmental Protection Agency and Bay Area Air Quality Management District through Contract 2016-129. I. C. F. was also supported by the California Agricultural Experiment Station, Hatch project CA-D-LAW-2229-H. The NASA AJAX project was also supported with Ames Research Center Director's funds and the support and partnership of H211; L. L. C. is gratefully acknowledged. J. E. M. and J.-M. R. were supported through the NASA Postdoctoral Program, and M. E. M. was funded through the Center for Applied Atmospheric Research and Education (NASA MUREP). We would like to thank Carol Bruegge, Brent Holben, and the rest of the AERONET staff for maintaining the network and their assistance with the data. We would also like to thank the anonymous reviewers for their helpful suggestions. We acknowledge the use of imagery from the NASA Worldview application (<https://worldview.earthdata.nasa.gov/>), part of the NASA Earth Observing System Data and Information System (EOSDIS). The CABOTS data are archived (at <https://www.esrl.noaa.gov/csd/projects/cabots/>). The views, opinions, and findings contained in this report are those of the author(s) and should not be construed as an official National Oceanic and Atmospheric

(83 ppbv) of 2016 on 27 July, and 22 of the 25 O₃ monitors in the SJVAB exceeded the 70-ppbv NAAQS on that day. PM_{2.5} was also enhanced at many of the SJVAB monitors on these days.

The increase in surface O₃ following the appearance of Soberanes smoke aloft suggests that the fire may have contributed to this increase. However, the week following the outbreak of the Soberanes Fire was also the hottest in the SJVAB during 2016 with daily maximum temperatures at the Fresno-Garland station reaching 41–42 °C (106–107 °F) on 27–29 July, compared to 34–36 °C (93–97 °F) on 18–22 July. Thus, the high O₃ and PM_{2.5} measured during that period may simply have been caused by more efficient photochemical production from locally emitted precursors (the smoke haze was not dense enough to significantly reduce the solar flux). Figure 14 plots the daily average PM_{2.5} and MDA8 O₃ measured by the Visalia N. Church St. and Fresno-Garland monitors as a function of daily maximum temperature (Jaffe et al., 2004). Parlier, where the highest O₃ was measured, did not measure PM_{2.5}. Figures 14a and 14c show that the highest daily average PM_{2.5} was measured in both Fresno and Visalia on 27 July when high β also appeared above the VMA. Neither of these daily averages approached the PM_{2.5} NAAQS of 35 μg/m³, but Figures 14b and 14d indicate that the O₃ NAAQS of 70 ppbv was exceeded by 13 ppbv in Visalia and 21 ppbv at Fresno-Garland on 27 July. Figures 14a and 14c show that the PM_{2.5} at both monitors was ~5 μg/m³ larger on 26–28 July than might be expected from the temperature dependence seen before the fire, but the ozone measurements in Figures 14b and 14d do not show a similar step increase. Indeed, Figure 14d shows that the highest MDA8 O₃ at the Fresno-Garland monitor (94 ppbv) was recorded on 1 July, well before the start of the fire. Also, while 26–28 July were three of the four highest MDA8 O₃ days in Visalia, the second highest day was 26 June with 79 ppbv. We conclude from these data that the contribution of the Soberanes Fire to the high O₃ measured in these two cities during late July and early August was a few ppbv at most, and certainly not the 13 and 21 ppbv by which the Visalia and Fresno-Garland monitors, respectively, exceeded the NAAQS on 27 July.

7. Summary and Conclusions

The outbreak of the Soberanes Fire during the 2016 CABOTS field campaign created a unique opportunity to study the spread of smoke and fire-generated O₃ into the SJVAB using coordinated remote sensing, ground-based lidar, and aircraft measurements. The ground-based NOAA TOPAZ lidar measurements show that ultraviolet backscatter profiles retrieved in the analysis of O₃ differential absorption lidar measurements can be useful as a tracer for fire smoke and help quantify O₃ production in dispersed fire plumes. The O₃-to-β ratio derived from the lidar measurements was found to decrease exponentially with smoke plume density, possibly because of the reduced actinic flux. Measurements of O₃, CH₄, and CO₂ by the Scientific Aviation and NASA AJAX aircraft suggest that CH₄ can be a good tracer for biomass burning in the free troposphere when CO measurements are unavailable, and comparisons between the lidar and aircraft show linear relationships between CH₄ and lidar backscatter. Both the lidar and aircraft measurements found O₃ enhancements of 40–60 ppbv of O₃ in the lower free troposphere above the Coast Ranges and eastern San Joaquin Valley but found no clear evidence that the fire significantly increased surface O₃ in the Fresno-Visalia area.

References

- Akagi, S. K., Craven, J. S., Taylor, J. W., McMeeking, G. R., Yokelson, R. J., Burling, I. R., et al. (2012). Evolution of trace gases and particles emitted by a chaparral fire in California. *Atmospheric Chemistry and Physics*, *12*(3), 1397–1421. <https://doi.org/10.5194/acp-12-1397-2012>
- Akagi, S. K., Yokelson, R. J., Wiedinmyer, C., Alvarado, M. J., Reid, J. S., Karl, T., et al. (2011). Emission factors for open and domestic biomass burning for use in atmospheric models. *Atmospheric Chemistry and Physics*, *11*(9), 4039–4072. <https://doi.org/10.5194/acp-11-4039-2011>
- Alvarez, R. J. II, Senff, C. J., Langford, A. O., Weickmann, A. M., Law, D. C., Machol, J. L., et al. (2011). Development and application of a compact, tunable, solid-state airborne ozone lidar system for boundary layer profiling. *Journal of Atmospheric and Oceanic Technology*, *28*(10), 1258–1272. <https://doi.org/10.1175/Jtech-D-10-05044.1>
- Avnery, S., Mauzerall, D. L., Liu, J. F., & Horowitz, L. W. (2011a). Global crop yield reductions due to surface ozone exposure: 1. Year 2000 crop production losses and economic damage. *Atmospheric Environment*, *45*(13), 2284–2296. <https://doi.org/10.1016/j.atmosenv.2010.11.045>

Administration or U.S. Government position, policy, or decision.

Avnery, S., Mauzerall, D. L., Liu, J. F., & Horowitz, L. W. (2011b). Global crop yield reductions due to surface ozone exposure: 2. Year 2030 potential crop production losses and economic damage under two scenarios of O₃ pollution. *Atmospheric Environment*, *45*(13), 2297–2309. <https://doi.org/10.1016/j.atmosenv.2011.01.002>

Bao, J. W., Michelson, S. A., Persson, P. O. G., Djalalova, I. V., & Wilczak, J. M. (2008). Observed and WRF-simulated low-level winds in a high-ozone episode during the Central California Ozone Study. *Journal of Applied Meteorology and Climatology*, *47*(9), 2372–2394. <https://doi.org/10.1175/2008jamc1822.1>

Bianco, L., Djalalova, I. V., King, C. W., & Wilczak, J. M. (2011). Diurnal evolution and annual variability of boundary-layer height and its correlation to other meteorological variables in California's Central Valley. *Boundary-Layer Meteorology*, *140*(3), 491–511. <https://doi.org/10.1007/s10546-011-9622-4>

Bonin, T. A., Carroll, B. J., Hardesty, R. M., Brewer, W. A., Hajny, K., Salmon, O. E., & Shepson, P. B. (2018). Doppler lidar observations of the mixing height in Indianapolis using an automated composite fuzzy logic approach. *Journal of Atmospheric and Oceanic Technology*, *35*(3), 473–490. <https://doi.org/10.1175/Jtech-D-17-0159.1>

Bryant, B. P., & Westerling, A. L. (2014). Scenarios for future wildfire risk in California: Links between changing demography, land use, climate, and wildfire. *Environmetrics*, *25*(6), 454–471. <https://doi.org/10.1002/env.2280>

Buysse, C. E., Kaulfus, A., Nair, U., & Jaffe, D. A. (2019). Relationships between particulate matter, ozone, and nitrogen oxides during urban smoke events in the Western US. *Environmental Science & Technology*, *53*(21), 12,519–12,528. <https://doi.org/10.1021/acs.est.9b05241>

Caputi, D. J., Faloona, I., Trousdell, J., Smoot, J., Falk, N., & Conley, S. (2019). Residual layer ozone, mixing, and the nocturnal jet in California's San Joaquin Valley. *Atmospheric Chemistry and Physics*, *19*(7), 4721–4740. <https://doi.org/10.5194/acp-19-4721-2019>

de Young, R. J., Grant, V. B., & Severance, K. (2005). Aerosol transport in the California Central Valley observed by airborne lidar. *Environmental Science & Technology*, *39*(21), 8351–8357. <https://doi.org/10.1021/es0487401>

Faloona, I. C., Chiao, S., Eiserloh, A. J., Alvarez, R. J. II, Kirgis, G., Langford, A. O., et al. (2020). The California Baseline Ozone Transport Study (CABOTS). *Bulletin of the American Meteorological Society*, BAMS-D-18-0302.1. <https://doi.org/10.1175/bams-d-18-0302.1>

Fast, J. D., Gustafson Jr, W. I., Berg, L. K., Shaw, W. J., Pekour, M., Shrivastava, M., et al. (2012). Transport and mixing patterns over central California during the carbonaceous aerosol and radiative effects study (CARES). *Atmospheric Chemistry and Physics*, *12*(4), 1759–1783. <https://doi.org/10.5194/Acp-12-1759-2012>

Gohm, A., Harnisch, F., Vergeiner, J., Obleitner, F., Schnitzhofer, R., Hansel, A., et al. (2009). Air pollution transport in an Alpine Valley: Results from airborne and ground-based observations. *Boundary-Layer Meteorology*, *131*(3), 441–463. <https://doi.org/10.1007/s10546-009-9371-9>

Holben, B. N., Eck, T. F., Slutsker, I., Tanré, D., Buis, J. P., Setzer, A., et al. (1998). AERONET—A federated instrument network and data archive for aerosol characterization. *Remote Sensing of Environment*, *66*(1), 1–16. [https://doi.org/10.1016/S0034-4257\(98\)00031-5](https://doi.org/10.1016/S0034-4257(98)00031-5)

Jaffe, D., Chand, D., Hafner, W., Westerling, A., & Spracklen, D. (2008). Influence of fires on O₃ concentrations in the western U.S. *Environmental Science & Technology*, *42*, 7.

Jaffe, D. A., Bertschi, I., Jaeglé, L., Novelli, P., Reid, J. S., Tanimoto, H., et al. (2004). Long-range transport of Siberian biomass burning emissions and impact on surface ozone in western North America. *Geophysical Research Letters*, *31*. <https://doi.org/10.1029/2004GL020093>

Jaffe, D. A., & Wigder, N. L. (2012). Ozone production from wildfires: A critical review. *Atmospheric Environment*, *51*, 1–10. <https://doi.org/10.1016/J.Atmosenv.2011.11.063>

Kochi, I., Champ, P. A., Loomis, J. B., & Donovan, G. H. (2012). Valuing mortality impacts of smoke exposure from major Southern California wildfires. *Journal of Forest Economics*, *18*(1), 61–75. <https://doi.org/10.1016/j.jfe.2011.10.002>

Kochi, I., Champ, P. A., Loomis, J. B., & Donovan, G. H. (2016). Valuing morbidity effects of wildfire smoke exposure from the 2007 Southern California wildfires. *Journal of Forest Economics*, *25*, 29–54. <https://doi.org/10.1016/j.jfe.2016.07.002>

Langford, A. O., et al. (2019). Intercomparison of lidar, aircraft, and surface ozone measurements in the San Joaquin Valley during the California Baseline Ozone Transport Study (CABOTS). *Atmospheric Measurement Techniques*, *12*(3), 1889–1904. <https://doi.org/10.5194/amt-12-1889-2019>

Leblanc, T., Brewer, M. A., Wang, P. S., Granados-Muñoz, M. J., Strawbridge, K. B., Travis, M., et al. (2018). Validation of the TOLNet lidars: The Southern California Ozone Observation Project (SCOOP). *Atmospheric Measurement Techniques*, *11*(11), 6137–6162. <https://doi.org/10.5194/amt-11-6137-2018>

Li, J., Mahalov, A., & Hyde, P. (2016). Impacts of agricultural irrigation on ozone concentrations in the Central Valley of California and in the contiguous United States based on WRF-Chem simulations. *Agricultural and Forest Meteorology*, *221*, 34–49. <https://doi.org/10.1016/j.agrformet.2016.02.004>

Lin, M. Y., A. M. Fiore, O. R. Cooper, L. W. Horowitz, A. O. Langford, H. Levy, et al. (2012). Springtime high surface ozone events over the western United States: Quantifying the role of stratospheric intrusions. *Journal of Geophysical Research*, *117*, D00v22. <https://doi.org/10.1029/2012jd018151>

Lin, M., Fiore, A. M., Horowitz, L. W., Cooper, O. R., Naik, V., Holloway, J., et al. (2012). Transport of Asian ozone pollution into surface air over the western United States in spring. *Journal of Geophysical Research*, *117*, D00v07. <https://doi.org/10.1029/2011JD016961>

National Interagency Coordination Center (2017). Wildland Fire Summary and Statistics Annual Report 2016Rep., 69 pp. Boise, ID.

Panek, J., Saah, D., Esperanza, A., Bytnerowicz, A., Fraczek, W., & Cisneros, R. (2013). Ozone distribution in remote ecologically vulnerable terrain of the southern Sierra Nevada, CA. *Environmental Pollution*, *182*, 343–356. <https://doi.org/10.1016/j.envpol.2013.07.028>

Park, R. J., Jacob, D. J., & Logan, J. A. (2007). Fire and biofuel contributions to annual mean aerosol mass concentrations in the United States. *Atmospheric Environment*, *41*(35), 7389–7400. <https://doi.org/10.1016/j.atmosenv.2007.05.061>

Peischl, J., Eilerman, S. J., Neuman, J. A., Aikin, K. C., de Gouw, J., Gilman, J. B., et al. (2018). Quantifying methane and ethane emissions to the atmosphere from central and western US oil and natural gas production regions. *Journal of Geophysical Research: Atmospheres*, *123*, 7725–7740. <https://doi.org/10.1029/2018jd028622>

Peischl, J., Ryerson, T. B., Holloway, J. S., Trainer, M., Andrews, A. E., Atlas, E. L., et al. (2012). Airborne observations of methane emissions from rice cultivation in the Sacramento Valley of California. *Journal of Geophysical Research*, *117*, n/a. <https://doi.org/10.1029/2012jd017994>

Pfister, G. G., Wiedinmyer, C., & Emmons, L. K. (2008). Impacts of the fall 2007 California wildfires on surface ozone: Integrating local observations with global model simulations. *Geophysical Research Letters*, *35*. <https://doi.org/10.1029/2008gl034747>

Potter, C. (2016). Landscape patterns of burn severity in the Soberanes Fire of 2016. *Journal of Geography and Natural Disasters*, *6*, 005. <https://doi.org/10.4172/2167-0587.S6-005>

- Pusede, S. E., & Cohen, R. C. (2012). On the observed response of ozone to NOx and VOC reactivity reductions in San Joaquin Valley California 1995-present. *Atmospheric Chemistry and Physics*, 12(18), 8323–8339. <https://doi.org/10.5194/acp-12-8323-2012>
- Pusede, S. E., et al. (2014). On the temperature dependence of organic reactivity, nitrogen oxides, ozone production, and the impact of emission controls in San Joaquin Valley, California. *Atmospheric Chemistry and Physics*, 14(7), 3373–3395. <https://doi.org/10.5194/acp-14-3373-2014>
- Rampanelli, G., Zardi, D., & Rotunno, R. (2004). Mechanisms of up-valley winds. *Journal of the Atmospheric Sciences*, 61(24), 3097–3111. <https://doi.org/10.1175/Jas-3354.1>
- Reid, J. S., Koppmann, R., Eck, T. F., & Eleuterio, D. P. (2005). A review of biomass burning emissions part II: Intensive physical properties of biomass burning particles. *Atmospheric Chemistry and Physics*, 5, 799–825. <https://doi.org/10.5194/acp-5-799-2005>
- Ryoo, J. M., Johnson, M. S., Iraci, L. T., Yates, E. L., & Gore, W. (2017). Investigating sources of ozone over California using AJAX airborne measurements and models.: Assessing the contribution from longrange transport. *Atmospheric Environment*, 155, 53–67. <https://doi.org/10.1016/j.atmosenv.2017.02.008>
- St. Clair, J. M., Swanson, A. K., Bailey, S. A., Wolfe, G. M., Marrero, J. E., Iraci, L. T., et al. (2017). A new non-resonant laser-induced fluorescence instrument for the airborne in situ measurement of formaldehyde. *Atmospheric Measurement Techniques*, 10(12), 4833–4844. <https://doi.org/10.5194/amt-10-4833-2017>
- Stein, A. F., Draxler, R. R., Rolph, G. D., Stunder, B. J. B., Cohen, M. D., & Ngan, F. (2015). NOAA'S HYSPLIT atmospheric transport and dispersion modeling system. *Bulletin of the American Meteorological Society*, 96(12), 2059–2077. <https://doi.org/10.1175/Bams-D-14-00110.1>
- Tanaka, T., Yates, E., Iraci, L. T., Johnson, M. S., Gore, W., Tadic, J. M., et al. (2016). Two-year comparison of airborne measurements of CO₂ and CH₄ with GOSAT at Railroad Valley, Nevada. *Geoscience and Remote Sensing. IEEE Transactions on*, 54(8), 4367–4375. <https://doi.org/10.1109/Tgrs.2016.2539973>
- Toon, O. B., Maring, H., Dibb, J., Ferrare, R., Jacob, D. J., Jensen, E. J., et al. (2016). Planning, implementation, and scientific goals of the Studies of Emissions and Atmospheric Composition, Clouds and Climate Coupling by Regional Surveys (SEAC(4)RS) field mission. *Journal of Geophysical Research: Atmospheres*, 121, 4967–5009. <https://doi.org/10.1002/2015jd024297>
- Trousdell, J. F., Caputi, D., Smoot, J., Conley, S. A., & Faloon, I. C. (2019). Photochemical production of ozone and emissions of NOx and CH₄ in the San Joaquin Valley. *Atmospheric Chemistry and Physics*, 19(16), 10,697–10,716. <https://doi.org/10.5194/acp-19-10697-2019>
- Trousdell, J. F., Conley, S. A., Post, A., & Faloon, I. C. (2016). Observing entrainment mixing, photochemical ozone production, and regional methane emissions by aircraft using a simple mixed-layer framework. *Atmospheric Chemistry and Physics*, 16(24), 15,433–15,450. <https://doi.org/10.5194/acp-16-15433-2016>
- U.S. Environmental Protection Agency (2014). Policy assessment for the review of the ozone National Ambient Air Quality Standards, *Rep. EPA-452/R-14-006*, Research Triangle Park, North Carolina.
- Urbanski, S. P. (2013). Combustion efficiency and emission factors for wildfire-season fires in mixed conifer forests of the northern Rocky Mountains, US. *Atmospheric Chemistry and Physics*, 13(14), 7241–7262. <https://doi.org/10.5194/acp-13-7241-2013>
- Westerling, A. L., Brown, T. J., Schoennagel, T., Swetnam, T. W., Turner, M. G., & Veblen, T. T. (2016). Climate and wildfire in western US forests. *Forest Conservation in the Anthropocene: Science, Policy, and Practice*, 43–55. <https://doi.org/10.5876/9781607324591.c003>
- Wettstein, Z. S., Hoshiko, S., Fahimi, J., Harrison, R. J., Cascio, W. E., & Rappold, A. G. (2018). Cardiovascular and cerebrovascular emergency department visits associated with wildfire smoke exposure in California in 2015. *Journal of the American Heart Association*, 7(8). <https://doi.org/10.1161/JAHA.117.007492>
- Wotawa, G., & Trainer, M. (2000). The influence of Canadian forest fires on pollutant concentrations in the United States. *Science*, 288(5464), 5.
- Yates, E. L., Iraci, L. T., Austerberry, D., Pierce, R. B., Roby, M. C., Tadic, J. M., et al. (2015). Characterizing the impacts of vertical transport and photochemical ozone production on an exceedance area. *Atmospheric Environment*, 109, 342–350. <https://doi.org/10.1016/j.atmosenv.2014.09.002>
- Yates, E. L., Iraci, L. T., Roby, M. C., Pierce, R. B., Johnson, M. S., Reddy, P. J., et al. (2013). Airborne observations and modeling of springtime stratosphere-to-troposphere transport over California. *Atmospheric Chemistry and Physics*, 13(24), 12,481–12,494. <https://doi.org/10.5194/Acp-13-12481-2013>
- Yates, E. L., Iraci, L. T., Singh, H. B., Tanaka, T., Roby, M. C., Hamill, P., et al. (2016). Airborne measurements and emission estimates of greenhouse gases and other trace constituents from the 2013 California Yosemite Rim wildfire. *Atmospheric Environment*, 127, 293–302. <https://doi.org/10.1016/j.atmosenv.2015.12.038>
- Yokelson, R. J., Andreae, M. O., & Akagi, S. K. (2013). Pitfalls with the use of enhancement ratios or normalized excess mixing ratios measured in plumes to characterize pollution sources and aging. *Atmospheric Measurement Techniques*, 6(8), 2155–2158. <https://doi.org/10.5194/amt-6-2155-2013>
- Yokelson, R. J., Christian, T. J., Karl, T. G., & Guenther, A. (2008). The tropical forest and fire emissions experiment: laboratory fire measurements and synthesis of campaign data. *Atmospheric Chemistry and Physics*, 8(13), 3509–3527. <https://doi.org/10.5194/acp-8-3509-2008>
- Zardi, D., & Whiteman, C. D. (2013). Diurnal mountain wind systems. In F. K. Chow, S. F. J. de Wekker, & B. J. Snyder (Eds.), *Mountain weather research and forecasting: Recent progress and current challenges*, (pp. 35–119). Dordrecht: Springer Netherlands. https://doi.org/10.1007/978-94-007-4098-3_2
- Zhong, S. Y., Whiteman, C. D., & Bian, X. D. (2004). Diurnal evolution of three-dimensional wind and temperature structure in California's Central Valley. *Journal of Applied Meteorology*, 43(11), 1679–1699. <https://doi.org/10.1175/Jam2154.1>

References From the Supporting Information

- Brioude, J., Cooper, O. R., Feingold, G., Trainer, M., Freitas, S. R., Kowal, D., et al. (2009). Effect of biomass burning on marine stratocumulus clouds off the California coast. *Atmospheric Chemistry and Physics*, 9(22), 8841–8856. <https://doi.org/10.5194/acp-9-8841-2009>
- Brioude, J., Cooper, O. R., Trainer, M., Ryerson, T. B., Holloway, J. S., Baynard, T., et al. (2007). Mixing between a stratospheric intrusion and a biomass burning plume. *Atmospheric Chemistry and Physics*, 7(16), 4229–4235.
- Di Giuseppe, F., S. Remy, P. Florian, and W. Fredrik (2016). Improving GFAS and CAMS biomass burning estimations by means of the Global ECMWF Fire Forecast system (GEFF), edited, ECMWF.
- Emanuel, K. A., & Zivkovic-Rothman, M. (1999). Development and evaluation of a convective scheme for use in climate models. *Journal of the Atmospheric Sciences*, 56, 1766–1782.

- Hanna, S. R. (1982). In F. T. M. Nieuwstadt, H. van Dop, & D. Reidel Publishing (Eds.), *Applications in air pollution modeling*, in *Atmospheric turbulence and air pollution modelling*. Company, Dordrecht: Holland.
- Malicet, J., Daumont, D., Charbonnier, J., Parisse, C., Chakir, A., & Brion, J. (1995). Ozone UV spectroscopy.2. Absorption cross-sections and temperature-dependence. *Journal of Atmospheric Chemistry*, *21*(3), 263–273. <https://doi.org/10.1007/Bf00696758>
- Muller, D., A. Ansmann, I. Mattis, M. Tesche, U. Wandinger, D. Althausen, and G. Pisani (2007). Aerosol-type-dependent lidar ratios observed with Raman lidar. *Journal of Geophysical Research*, *112*(D16). <https://doi.org/10.1029/2006jd008292>
- Murayama, T., Muller, D., Wada, K., Shimizu, A., Sekiguchi, M., & Tsukamoto, T. (2004). Characterization of Asian dust and Siberian smoke with multiwavelength Raman lidar over Tokyo, Japan in spring 2003. *Geophysical Research Letters*, *31*, Artn L23103. <https://doi.org/10.1029/2004gl021105>
- Proffitt, M. H., & Langford, A. O. (1997). Ground-based differential absorption lidar system for day or night measurements of ozone throughout the free troposphere. *Applied Optics*, *36*(12), 2568–2585.
- Stohl, A., Forster, C., Frank, A., Seibert, P., & Wotawa, G. (2005). Technical note: The Lagrangian particle dispersion model FLEXPART version 6.2. *Atmospheric Chemistry and Physics*, *5*, 2461–2474.
- Völger, P., Bösenberg, J., & Shult, I. (1996). Scattering properties of selected model aerosols calculated at UV-wavelengths: Implications for DIAL measurements of tropospheric ozone. *Contributions to Atmospheric Physics*, *69*, 177–187.